P–T evolution of eclogite-facies metabasite from NE Sardinia, Italy: Insights into the prograde evolution of Variscan eclogites

P-T evolution of eclogite-facies metabasite from NE Sardinia, Italy: insights into the prograde evolution of Variscan eclogites

Gabriele Cruciani[a], Marcello Franceschelli[a], Chiara Groppo[b]

[a] *Dipartimento di Scienze della Terra, Via Trentino 51, Università degli Studi di Cagliari, I-09127, Cagliari, Italy*
[b] *Dipartimento di Scienze Mineralogiche e Petrologiche, Università degli Studi di Torino, via Valperga Caluso 35, 10125 Torino, Italy*

ABSTRACT

A petrological study of the Punta Orvili metabasite in NE Sardinia has been carried out, integrating quantitative pseudosection modelling with reaction balancing, with the aim of reconstructing the metamorphic evolution and P-T path.

The Punta Orvili metabasite preserves microstructural evidence of: (i) a pre-symplectite polyphase and prograde stage (M1) indicated by the occurrence of amphibole inclusions in garnet, by Na-rich diopside and by compositional zoning in garnet, clinopyroxene and amphibole; (ii) a symplectite stage (M2) represented by the occurrence of Cpx_2+ Pl_1 symplectite; (iii) a corona stage (M3) documented by the formation of micrometre-thick Pl_2 ± Am_3 ± Ilm coronas around garnet; (iv) a late stage (M4), documented by the growth of epidote and albite and by the replacement of biotite and clinopyroxene by chlorite. The M1 pre-symplectite stage has been modelled by P-T pseudosections calculated in the NCKFMASTH model system at a_{H2O}=1 (for a_{H2O} = 0.5 temperature values are ~50°C lower). Mg and Ca zoning in garnet and Na zoning in clinopyroxene testify to a progressive increase in temperature and pressure during garnet and clinopyroxene growth from 610 < T < 630°C, 1.7 < P <1.8 GPa up to 620 < T < 650°C, 1.9 < P <2.1 GPa, allowing to reconstruct a prograde segment of the P-T path. Peak pressure conditions were reached in the amphibole-eclogite facies field. Destabilization of clinopyroxene led to the formation of Cpx_2 + Pl_1 symplectite (M2 stage) at P-T conditions of 760 < T < 800°C, 0.9 < P < 1.0 GPa.

The corona stage (M3) was modelled in the NCKFMASTH model system using the bulk composition of the effectively reacting microdomain, calculated from mineral compositions and stoichiometric coefficients of the corona-forming reaction. T = 610-670°C and P ~ 0.7 GPa have been determined for this stage. Presumed P-T conditions of the latest re-equilibration stage (M4 stage) are around 300-400°C and 0.2-0.3GPa.

The prograde evolution of the Punta Orvili metabasite took place under a geothermal gradient of ~10-13 °C/km, compatible with a relatively hot subduction of a small, young marginal basin. Subsequent increase of the geothermal gradient up to 25-30°C/km suggests that subduction was followed by the Variscan continental collision.

The P-T path of the Punta Orvili metabasite has significant analogies with that of the retrogressed eclogite of Golfo Aranci, NE Sardinia, and with other eclogites from the

Migmatite Complex of NE Sardinia. These rocks underwent a fairly similar metamorphic evolution resulting from an oceanic subduction followed by continental collision.

Keywords: metabasite, metamorphic evolution, pseudosection modelling, P-T path, Sardinia, Variscan Orogeny.

1. Introduction

Over the last two decades the reconstruction of the prograde P-T path in eclogites has been receiving a great deal of attention, as it provides an insight into thermal and metamorphic evolution of palaeosubduction zones. The detailed investigation of the prograde evolution of eclogites was initially based on: the identification of prograde assemblages preserved as inclusions in garnet and/or omphacite (e.g. Pognante et al., 1980; Möller, 1998, 1999), and thermobarometry applied to mineral inclusions (e.g. Clarke et al., 1997; Carson et al., 1999; Elvevold and Gilotti, 2000; Page et al., 2003; Štípská et al., 2005) and/or zoned minerals (e.g. O'Brien and Vràna, 1995 ; O'Brien, 1997; Marmo et al., 2002; Štípská et al., 2005; Endo et al., 2009). More recently, improvements in thermodynamic databases and solid solution models (e.g. Green et al., 2007; White et al., 2007) and the development of methods that account for the possible fractionation of bulk composition due to the growth of garnet porphyroblasts (e.g. Stüwe, 1997; Marmo et al., 2002; Evans, 2004; Zuluaga et al., 2005; Gaidies et al., 2006; Groppo and Rolfo, 2008), have increased the popularity of thermodynamic modelling (i.e. pseudosections) for reconstructing the prograde P-T trajectories of eclogites (e.g. Wei et al., 2003, 2009; Štípská et al., 2005, 2006; Groppo et al., 2007, 2009; Powell and Holland, 2008).

In the Variscan terranes a prograde metamorphic evolution has been reported for eclogites from many locations, including for example the Bohemian Massif (e.g. O'Brien, 1997; Štípská et al., 2005, 2006), South Carpathians, Romania (e.g. Medaris et al., 2003), Savona crystalline massif of Italy (e.g. Messiga et al., 1991), Gföhl Unit of the Moldanubian Zone (e.g. Faryad et al., 2010).

Although eclogites are not common in the Variscan chain of Sardinia (only four major sites - the most widely studied are Punta de li Tulchi and Golfo Aranci outcrops, see Franceschelli et al., 2007 for a review), a prograde metamorphic history has also been suggested for some of these rare eclogite occurrences. Following the study by Miller et al. (1976), Franceschelli et al. (1998, 2007) suggested that a pre-eclogite stage is preserved in the Punta de li Tulchi eclogite based on the findings of tschermakite and zoisite relics entrapped in garnet porphyroblasts. A prograde stage has also been suggested by Giacomini et al. (2005) for the Golfo Aranci eclogites. These authors attributed edenite-andesine inclusions preserved in kyanite porphyroblasts to a prograde, pre-eclogitic metamorphism that occurred under amphibolite-facies P-T conditions. In the metabasite from Punta Orvili the zoning patterns of clinopyroxene and garnet porphyroblasts (i.e. Na increasing towards the clinopyroxene rim; Ca decreasing and Fe and Mg increasing toward the garnet rim) preliminarily suggested that these rocks recorded a prograde portion of their metamorphic history in the eclogite-facies (Franceschelli et al., 2007). Currently available data on the P-T evolution of Sardinian eclogites have been obtained chiefly from conventional thermobarometry (Franceschelli et al., 1998, 2007; Cortesogno et al., 2004) and/or Thermocalc Average PT methods (Giacomini et al., 2005) applied on peak and prograde assemblages, whereas the pseudosection approach has never been applied so far.

The focus of this paper is on the poorly studied Punta Orvili metabasite, which differs from the other well studied Sardinian eclogites for a number of reasons: (i) geochemical data suggest that the igneous protolith of the Punta Orvili metabasite has an alkaline affinity (Cruciani et al., 2010), whereas all the other Sardinian eclogites are MORB-type tholeiites (Cappelli et al., 1992); (ii) the Punta Orvili metabasite is among the few Sardinian eclogites that do not contain orthopyroxene, whereas the more widely studied Punta de li Tulchi and Golfo Aranci eclogites are orthopyroxene-bearing rocks (Franceschelli et al., 2007); (iii) the Punta Orvili metabasite belongs to the Low to Medium Grade Metamorphic Complex of Carmignani et al. (1992) or Hercynian Metamorphic Complex with Dominant Amphibolite Assemblages of Carmignani et al., 2001).

A detailed petrological study of the Punta Orvili metabasite has been performed by integrating quantitative pseudosection modelling and reaction balancing, with the aim to: (i) reconstruct, using the most recent petrologic approaches, the metamorphic evolution and P-T path of a still poorly investigated Sardinian eclogite; (ii) compare the P-T evolution of the Punta Orvili metabasite with the other eclogites from northern

Sardinia; (iii) discuss the obtained P-T history of Punta Orvili metabasite in the context of the Variscan chain of Sardinia.

2. Geological setting

2.1. The Variscan chain of Sardinia

The Variscan chain of Sardinia is a branch of the southern European Variscides. From South to North, it has been classically divided into an External Zone (SW Sardinia), a Nappe Zone (central Sardinia) and an Axial or Internal Zone (northern Sardinia). The latter is further divided into the Migmatite Complex and the Low to Medium Grade Metamorphic Complex respectively North and South of the Posada-Asinara Tectonic Line (Carmignani et al., 1992, 2001) (Fig. 1). In southern and central Sardinia the degree of Variscan metamorphism changes progressively from very low to low grade, whereas in northern Sardinia (Axial Zone) it varies from low to high grade, reaching the sillimanite + K-feldspar grade north-eastwards.

The metamorphic basement of north Sardinia underwent a polyphase Variscan deformation. Up to five (D_1 to D_5) deformation phases have been recognized (Franceschelli et al.2005, Helbing et al. 2006 and references therein). The D_1 phase produced S_1 schistosity recognizable as rare intrafoliar folds (Elter et al., 1986) transposed and overprinted by the D_2 deformation. The D_2 phase generated the most evident structures in the Migmatite Complex, i.e. folds with E–W trending axes accompanied by S_2 axial plane schistosity. D_2 has been considered a transpressional deformation by Carosi and Palmeri (2002). The D_3 phase, gently superimposed on the previous D_2, produced open folds with spaced cleavages, in the South, and pervasive schistosity locally, North of Olbia. The D_4 phase is mainly restricted to the cataclastic, mylonitic rocks cropping out in the Posada Valley shear zone, where C-type shear band crenulation cleavages were generated by non coaxial-shearing. In the same shear zone, the D_5 deformation gave rise to a large flexure parallel to the orogenic trend, as witnessed by the uplift of the Axial Zone with respect to the schistose envelope (Helbing et al., 2006). More details on metamorphism and deformation in the Axial Zone can be found in the extended review of Variscan orogeny in Sardinia by Franceschelli et al. (2005) and the recent paper of Elter et al. (2010).

2.2. Eclogite occurrences in northern Sardinia

Metabasites with eclogite-facies relics have been found in the high-grade gneisses of the Migmatite Complex and in the medium-grade gneisses of the Low to Medium Grade Metamorphic Complex. The two occurrences of eclogitic rocks were described as eclogite A and eclogite B respectively by Cortesogno et al. (2004).

In the Migmatite Complex the eclogitic rocks occur as boudins parallel to, and enveloped by, the E-W striking S_2 schistosity. Except for the hectometre-size bodies and lenses cropping out at Golfo Aranci, Punta Tittinosu and Punta de li Tulchi, most of the eclogites from the Migmatite Complex are metre-sized (Franceschelli et al., 2007). Most of the eclogites from the Migmatite Complex studied so far contain orthopyroxene.

The metabasites from the Low to Medium Grade Metamorphic Complex occur as decametre size lenses and boudins in gneiss and mylonitic gneiss of Asinara Island, Anglona, and along the Posada Valley shear Zone. However, only the metabasites from Anglona retain relics of eclogite-facies assemblages (Cortesogno et al., 2004). Orthopyroxene has not been observed up to now in the eclogites hosted in the medium-grade gneisses.

The protoliths of Sardinian eclogites are mostly MORB-type tholeiites (Cappelli et al., 1992), as evidenced by their slightly convex LREE patterns, slightly negative Eu anomaly and flat HREE patterns, except for the metabasite from Punta Orvili that exhibited an alkaline affinity (Cruciani et al., 2010).

Different stages have been recognised in the evolution of eclogites from Sardinia. In particular, Franceschelli et al. (1998) recognised five stages in the Punta de li Tulchi retrogressed eclogites, which are also discussed by Giacomini et al. (2005) for the Golfo Aranci eclogites: (i) a pre-eclogitic stage under amphibolite-facies conditions; (ii) a peak-P eclogite stage documented by the occurrence of omphacite relics in garnet; (iii) a granulite stage characterized by the growth of Px + Pl (abbreviations according to Fettes and Desmons, 2007) symplectites after omphacite; (iv) an amphibolite stage with the development of amphibole + plagioclase coronas around garnet, and (v) a greenschist to sub-greenschist stage characterized by the growth of actinolite, chlorite, epidote, titanite, sericite, and rare prehnite.

Regarding the geochronological data on Sardinian eclogites, Palmeri et al. (2004) found U–Pb zircon ages in the Punta de li Tulchi eclogite giving three weighted means of 453 ± 14, 400 ± 10 and 327 ± 7 Ma. The first age was interpreted as the protolith age, the second was considered as the likely age of the HP eclogitic event or the result of Pb loss during the main Variscan event, while the third was attributed to the final retrogression to amphibolite facies conditions. Magmatic zircons from the Golfo Aranci eclogites yielded a mean age of 460 ± 5 Ma, interpreted as the protolith age by Giacomini et al. (2005a). This value fits well with the protolith age of 453 ± 14 Ma found by Palmeri et al. (2004) and with the 457 ± 2 Ma obtained by Cortesogno et al. (2004) for type-A eclogite. In addition, in type-A eclogite, Cortesogno et al. (2004), defined an age of 403 ± 4 Ma from a second zircon population, interpreted as dating the zircon crystallization during the high-grade event.

In zircons recovered from eclogites of the Migmatite Complex, Giacomini et al. (2005b) found metamorphic ages clustering around Early Visean (~345 Ma) and between Late Visean (~325 Ma) and 300 Ma. The first cluster was interpreted as the age of the HP eclogitic event, whereas the second was attributed to post-HP amphibolitic re-equilibration.

2.3. The Punta Orvili metabasite

The Punta Orvili outcrop is located near the southern edge of the Migmatite Complex, on the northern side of the Posada Valley Shear Zone (Fig. 1). The Punta Orvili rocks consist of a sequence of mostly mylonitic gneiss, with widespread calc-silicate nodules and rare lenses of metabasite with eclogite-facies relics (Elter, 1987). The main foliation observable in the field is the S_2 schistosity striking N 60-80° and dipping 30°-50° toward SE, related to the D_2 regional deformation event. Locally, the S_2 schistosity is transposed by centimetre size, sinistral strike-slip green-schist shear zones (S_3), striking N 30° and dipping 60° SE. Three mineral lineations have been recognized in the XY plane of the S_2 schistosity in mylonitic gneiss: a feldspar + Qtz lineation striking N30° - 50° and dipping 20°-30° SW; a Qtz lineation striking N 40°, dipping 30° SW; a Bt ± Chl lineation striking N 20° and dipping 15°-30° SW. The mylonitic gneiss is characterized by millimetre to centimetre size quartz-feldspathic domains, sometimes characterized by polygonal microstructure, enveloped by the S_2 foliated phyllosilicaterich matrix. The matrix consists of abundant muscovite, biotite, chlorite and fibrolite in various combinations (Cruciani et al., 2007). Chlorite and fibrolite define the main rock foliation, whereas muscovite occurs as medium-grained elongated flakes aligned in the foliation or as late coarse-grained flakes overgrown on the main foliation and locally preserving inclusions of fibrolite needles. Biotite, where present, is aligned along the rock foliation and is partially fibrolitized.

The Punta Orvili metabasite crops out as a main lens of roughly 8-10 m in diameter, enveloped by the S_2 schistosity of the surrounding mylonitic gneisses. A recent geological survey in the area revealed the occurrence of a few metre-sized boudins cropping out very near to the main metabasite lens. This lens consists of dark, massive rocks with rounded millimetre-size garnet. Centimetre to decimetre-size late shear zones are sometimes recognisable within the metabasite. The contact between the metabasite lens and the surrounding mylonitic gneiss is marked by centimetre-thick band of ultramylonitic gneiss with N110°-striking, 53° SW dipping S_2 schistosity.

3. Petrography

The Punta Orvili metabasite consists of amphibole (~ 40 vol%), garnet (~ 25 vol%), clinopyroxene (~ 10 vol%), biotite (~ 12-13 vol%), ilmenite and Fe-oxide (up to 10 vol%) and plagioclase (<2-3 vol%) (Figs. 2a, b). Minor titanite, apatite, rutile, quartz, epidote, chlorite and rare K-feldspar have also been observed. It has homogeneous composition with narrow ranges of variability for the major oxides: SiO_2 = 44.89-47.57 (wt%), TiO_2 = 2.4-2.8, Fe_2O_{3tot} = 13.2-15.1, MnO = 0.18-0.23, and CaO = 11.06-12.30. Na_2O and K_2O range from 0.75-1.38 and 0.54-0.88, respectively. Worthy of note is the high MgO (12.94-14.35 wt%) and low Al_2O_3 (7.53-9.59 wt%) contents (Cruciani et al., 2010).

The most important textural feature of the Punta Orvili metabasite is the occurrence of clinopyroxene + plagioclase symplectites (Figs. 2a, b) as well as plagioclase-amphibole coronitic assemblages (Figs. 3a, c, d, f) around garnet, as commonly observed in several metabasite lenses with eclogite facies relics from NE Sardinia (Franceschelli et al., 1998, 2007).

Clinopyroxene occurs as millimetre-size, strongly fractured crystals (Cpx_1) containing tiny quartz needles in the core (Fig. 3a) and showing equilibrium contacts with the large amphibole crystals (Am_1) (Fig. 2c). Clinopyroxene also occurs as fine-grained Cpx_2 forming symplectite microstructures with plagioclase (Pl_1) (Figs. 3c, e), commonly growing at the expense of Cpx_1 (Figs. 2b, d and 3c,e). The size, shape and orientation of the Cpx_2 vary significantly: very fine grained crystals do not show any particular orientation, whereas those with a slightly coarser grain size seem to radiate from the partially replaced Cpx_1.

Garnet occurs as strongly fractured and embayed grains up to 1-1.5 mm in size (Figs. 3a, b, c, d). Inclusions in garnet are amphibole (Am_1), clinopyroxene (Cpx_1), rutile, zircon and rounded apatite. Plagioclase occurs as micrometre-size crystals (Pl_1) in the symplectites (Figs. 2c, e) or as coronitic shells (Pl_2) growing with amphibole and/or ilmenite around garnet (Figs. 2c, e). No plagioclase crystals or relics other than these two textural occurrences have ever been found. Biotite abundance varies widely from one sample to another. It occurs as randomly–oriented, brown flakes a few hundred microns in length, partially replaced by chlorite (Figs. 3c, e, f). Inclusions in biotite are mostly zircon grains up to a few hundred microns in size.

Amphibole is by far the most abundant mineral in the Punta Orvili metabasites. It has been observed in four main textural occurrences (i.e. Am_1-Am_4): (i) Am_1 occurs as colourless to pale-green/pale-brown amphibole in the matrix, or as rounded inclusions in garnet (Figs. 2e, f and 3d). Most Am_1 crystals in the matrix show irregular and discontinuous zoning defined by an inclusion-rich brown actinolitic core, surrounded by an inclusion-free, colourless hornblende rim (Fig. 3b). Micrometre size inclusions in the core consist mostly of aligned rutile (Fig. 3e) and rare quartz, biotite, and clinopyroxene; (ii) Am_2 occurs as a thin layer, similar to a halo, at the contact between Am_1 and the coronitic shell around garnet (Fig. 3b); (iii) Am_3 grows in discontinuous blebs and droplets together with plagioclase and/or ilmenite in the coronitic microstructures around garnet (Figs. 3a, c, d, f); (iv) anhedral Am_4 occurs in veins and fractures cutting the rock foliation.

Very rare quartz locally occurs in the rock matrix or as tiny needles in the core of Cpx_1. Ilmenite, rutile and titanite form complex intergrowths. Rutile is surrounded by ilmenite and both rutile and ilmenite are, in turn, surrounded by micrometre-thick shells of titanite. Titanite also grows as fibrous, micron-sized needles along the cleavages of biotite. Epidote occurs as scattered and zoned grains. Chlorite mostly grows at the expense of biotite and in the fractures of clinopyroxene and garnet. Minor K-feldspar is also present in the late amphibole + titanite veins.

4. Mineral chemistry

The chemical composition of minerals from three metabasite samples (PO2, U126, PO6) was determined with a fully automated Cameca SX 50 electron microprobe at the IGAG-CNR Roma. Operating conditions were 15 kV accelerating voltage, a beam current of 15 nA and a 5-10 µm variable spot size. Natural and synthetic wollastonite, olivine, corundum, magnetite, rutile, orthoclase, jadeite, pure Mn, pure Cr, fluoro-phlogopite, and baryte were used as standards. Microstructural study, BSE imaging, and additional EDS analyses were performed with an FEI Quanta 200 SEM equipped with an EDAX-EDS detector at Cagliari University. Selected microprobe analyses of amphibole, garnet, clinopyroxene, plagioclase, biotite and ilmenite are reported in Table 1 and in Tables 1A and 2A of supplementary material.

Structural formulae have been calculated on the basis of 6, 12 and 8 oxygens for clinopyroxene, garnet and plagioclase, respectively. Fe^{3+} content has been calculated from charge balance for clinopyroxene and according to Droop (1987) for garnet, whereas all iron has been assumed to be divalent in biotite. Amphibole structural formula has been calculated using the Amph-IMA Program with 23 oxygens and a normalization scheme according to Mogessie et al. (2004).

Clinopyroxene: Granoblastic Cpx_1 is a diopside (Fig. 4) with X_{Mg} [Mg/(Mg+Fe^{2+})] = 0.80 - 0.87. Compositional traverse (Fig. 5) across Cpx_1 reveals a zoning characterized by Na increasing toward the rim, counterbalanced by a decrease in Ca. X_{Na} [Na/(Na+Ca)] ranges between 0.07-0.18 in the three samples, with the strongest variability between core and rim observed for sample PO2 (X_{Na}=0.14 in the core and 0.18 in the rim). No significant variability in the X_{Mg} has been observed from core to rim. The rare clinopyroxene inclusions preserved in the garnet core show a composition similar to the Cpx_1 core. Cpx_2 from the symplectite is also a diopside (Fig. 4) and differs from Cpx_1 for the lower Na content (X_{Na} = 0.06-0.08).

Garnet is almandine-rich (Alm=49-55 mol%) and spessartine-poor (Sps=1.4-2.2 mol%), with intermediate pyrope and grossularite contents ranging between 17-26 mol% and 17-31 mol%, respectively. Compositional traverse (Fig. 6) across a garnet grain reveals irregular zoning with a systematic decrease in Ca (0.83-0.93 a.p.f.u. in the core, 0.51-0.58 a.p.f.u. in the rim), counteracted by an increase in Fe (1.44-1.51 a.p.f.u. in the core, 1.57-1.65 a.p.f.u. in the rim) and Mg (0.53-0.56 a.p.f.u. in the core, 0.69-0.75 a.p.f.u. in the rim) from core to rim. Mn is constant, or irregularly variable with a very slight enrichment in the outermost rim (Fig. 6).

Plagioclase: Pl_1 lamellae from the symplectites are mostly andesine (An_{30-40}), more rarely oligoclase. Pl_2 from the coronitic shell around garnet is more calcic with compositions in the andesine-labradorite range (An_{47-51}). Orthoclase content is very low, and trace amounts of Fe, Mn, Mg, and Ba have also been found in both Pl_1 and Pl_2. Albite lamellae (Pl_3) replacing Pl_1 have been found locally in the symplectite.

Biotite is Ti- and Ba-rich. TiO_2 content is up to 5 wt% (Ti: 0.6 a.p.f.u.) while BaO is up to 3 wt% (Ba: 0.2 a.p.f.u.). X_{Mg} ratios are mostly comprised between 0.63 and 0.66.

Amphiboles in all the microstructural sites are calcic (Fig. 8) according to the classification by Leake et al. (1997). In order of decreasing abundance, Am_1 consists of: i) unzoned actinolite grains (Al = 0.4-0.6 a.p.f.u.; Si = 7.6-7.8 a.p.f.u.); ii) zoned grains with an actinolitic core and a Mg-hornblende rim (see Figs. 7, 8 and Table 1); iii) unzoned Mg-hornblende grains. The increase in Ti, Al, Ca, Na, and K contents from core to rim in Am_1 is counterbalanced by Si and Mg decrease (Fig. 7). Am_1 included in garnet is mainly a Mg-hornblende, with Al = 0.7-1.0 a.p.f.u. and Si = 7.3-7.6 a.p.f.u., i.e. with Si content lower than that of the Am_1 core. Am_2 is a pargasite to tschermakite, and differs from Am_1 for the lower Si and Mg and higher Al, Na, and K contents. Coronitic droplets of Am_3 varying in composition between Mg-hornblende, tschermakite and pargasite are very similar to Am_2. Am_4 occurring in late veins is an actinolite.

5. Metamorphic evolution and reaction history

The Punta Orvili metabasites preserve microstructural evidence of a pre-symplectite stage (M1), a symplectite stage (M2), a corona stage (M3), and a late retrograde stage (M4). The metamorphic evolution inferred from microstructural relationships is summarized in Fig. 9.

5.1. M1 pre-symplectite stage

A pre-symplectite prograde stage is evidenced by: (i) the widespread occurrence of amphibole (Am_1) inclusions in garnet; (ii) Na-rich diopside (Cpx_1) crystals with symplectite overgrowth in the rock matrix, and (iii) garnet and clinopyroxene compositional zoning. Mineral inclusions in garnet and clinopyroxene suggest that the stable mineral assemblage during early M1 stage was Cpx_1 (core) + Grt (core) + Am_1 (included in garnet) + Rt + Qtz. Core-rim zoning patterns of garnet and Cpx_1 reflect the transition from the early M1 stage (M1c in Fig. 9) to a later M1 stage (M1r) characterized by the assemblage Cpx_1 (rim) + Grt (rim) + Am_1 in the matrix + Rt + Qtz. We tentatively attribute to the prograde M1 stage also the Ti- and Ba-rich biotite (Fig. 9).

5.2. M2 symplectite stage

This stage is documented by the occurrence of Cpx_2+ Pl_1 symplectites. The observation that symplectites grow at the margin of Cpx_1 is the best evidence of the role played by Cpx_1 in the symplectite-forming reaction. Reaction modelling by the least square-method (CSpace version 1.01, Djinn Works) applied to the composition of Cpx_1 rim, quartz, symplectitic plagioclase (Pl_1) and clinopyroxene (Cpx_2) from sample PO2 (mineral compositions in Table 1) resulted in the following balanced reaction, which accounts for the formation of Pl_1 + Cpx_2 symplectites:

(1) 0.756 Cpx_1 (rim) + 0.015 Qtz = 0.086 Pl_1 + 0.648 Cpx_2

Residuals are reported in the Appendix. Reaction (1) is consistent with the observed microstructures, in that Cpx_1 and quartz are reactants and symplectitic minerals (Pl_1, Cpx_2) are products. Reaction (1) is also validated by the relative volumes of the reactants and products calculated from the stoichiometric coefficients and tabulated molar volumes reported in the literature (Helgeson et al., 1978). According to reaction (1), in fact, the symplectite would have resulted in 83 vol% Cpx_2 and 17 vol% Pl_1, which is similar to the proportion estimated in selected symplectitic microdomains of sample PO2 (Figs. 2c, e).

Balancing a reaction, however, is generally an over-determined problem, since there are usually more independent equations than independent variables, at least if we assume that the system was closed (Godard and Martin, 2000). This means that, although the balanced reaction (1) is consistent with microstructural observations, it likely represents only one end-member of an infinity of plausible reactions, all playing a role in the formation of the Cpx_2+ Pl_1 symplectites. The local occurrence of Cpx_2+ Pl_1 symplectites replacing Cpx_1 and protruding from Am_1 (Fig. 2d), for example, suggests that the symplectite-forming reaction may be more complex than reaction (1), likely involving also Am_1 between the reactants. This further suggests that the chemical domain involved in the symplectite formation is larger than the microstructural site actually occupied by the symplectite.

5.3 .M3 corona stage

This stage is dominated by the development of micrometre-thick Pl_2 ± Am_3 ± ilmenite coronas around garnet. Am_2, which has the same composition as Am_3 (see Table 1 and Fig. 8) but occurs in different microstructural sites, has also been attributed to this stage. The occurrence of Am_3 and Pl_2 in coronitic assemblages at the garnet/symplectite interfaces (see Figs. 2 and 3c, d) suggests that the corona results from the reaction between garnet rim and symplectite minerals (Pl_1, Cpx_2). The following balanced reaction has been modelled using the composition of garnet rim, symplectitic minerals and the prevalent composition of Am_3 (Mg-Hbl):

(2) 0.286 Grt rim + 0.460 Pl_1 + 0.224 Cpx_2 + 0.354 rutile + 0.144 H_2O = 0.143 $Am_{2,3}$ + 0.617 Pl_2 + 0.329 Ilm

Residuals for reaction (2) are generally low (see Appendix). However, slightly high Na residuals have been obtained for garnet, plagioclase, and clinopyroxene, suggesting minor changes in composition for Na-bearing phases during the corona-forming reaction. Variability in composition of Am_2 and Am_3 was probably controlled by the diffusion and initial distribution of Si and Al in the reacting microdomain.

5.4. M4 late stage

This stage is poorly constrained and is documented by the local growth of epidote and albite, by the replacement of biotite and clinopyroxene by chlorite, and by the formation of veins and fractures filled with actinolitic amphibole, titanite and minor K-feldspar. Titanite growth along the cleavages of biotite and around ilmenite and rutile can also be related to this stage.

6. *P-T* pseudosection modelling

The metamorphic evolution of the Punta Orvili metabasite has been constrained using the petrologic approach of isochemical phase diagrams. P-T pseudosections were calculated using PerpleX_09 (Connolly, 1990, 2009) and the internally consistent thermodynamic data set and the equation of state for H_2O by Holland and Powell (1998, revised 2004). The phases considered in the calculation were: plagioclase, quartz, orthopyroxene, clinopyroxene, garnet, biotite, phengite, amphibole, chlorite, zoisite, clinozoisite, lawsonite, rutile, ilmenite and titanite. Solid-solution models are those of Holland and Powell (1998) for garnet and phengite, Holland and Powell (1996) for orthopyroxene, Green et al. (2007) for clinopyroxene, Holland et al. (1998) for chlorite and Dale et al. (2005) for amphibole.

6.1. Modelling of stages M1 and M2

The first stages of the metamorphic evolution (M1 and M2) have been modelled using a P-T pseudosection calculated in the NCKFMASTH model system using the bulk composition of sample PO2 (SiO_2=47.51, TiO_2=2.43, Al_2O_3=8.76, FeO=11.99, MgO=13.48, CaO=11.16, Na_2O=1.38, K_2O=0.83 wt%). All Fe was assumed to be Fe^{2+}, because Fe^{3+}-bearing oxides are absent, epidote is a very minor phase belonging to the retrograde assemblage, and the Fe^{3+} content in the main mafic minerals (garnet, amphibole, clinopyroxene, biotite) is negligible (see Table 1). Since garnet contains low spessartine component (MnO < 1wt%), MnO was also neglected in the model system. H_2O was treated as a perfectly mobile component and pseudosections were calculated at both a_{H2O} = 0.5 and a_{H2O} = 1.0 to test the influence of water activity on the stability of the metamorphic assemblages (see further discussion).

The P-T pseudosection calculated at a_{H2O} = 1.0 is shown in Fig. 10. It is dominated by quadri- and tri-variant fields, with hexa- and pentavariant fields confined at LT-LP conditions. According to this topology, the prograde, plagioclase-free, pre-symplectite assemblage M1, consisting of Cpx_1+Grt+Am_1+Rt+Qtz±Bt is modelled by the Cpx+Bt+Am+Grt+Rt±Ilm±Chl tri- and quadri-variant fields, stable at P>1.4 GPa and T<790°C (chlorite is present in very minor amounts in these fields). Further constraints can be obtained from the clinopyroxene, amphibole and garnet compositional isopleths (Fig. 11). Comparison of the modelled isopleths of X_{Na}(Cpx) (Fig. 11a), Si content in amphibole (Fig. 11b), X_{Ca}(Grt) and X_{Mg}(Grt) (Figs. 11c, d) with the mineral compositions actually determined in sample PO2 (Table 1) allowed to restrict P-T conditions of the prograde stage, and to distinguish:

(a) an early prograde M1 stage (M1c), defined by the composition of Cpx_1 core (X_{Na} = 0.13-0.15), Am_1 included in garnet (Si = 7.3-7.6 a.p.f.u.) and Grt core (X_{Ca} = 0.27-0.31; X_{Mg} = 0.17-0.20), at T=610-630°C, P=1.7-1.8 GPa;

(b) a late M1 stage (M1r), defined by the composition of Cpx_1 rim (X_{Na} = 0.17-0.19), Grt rim (X_{Ca} = 0.17-0.21 ; X_{Mg} = 0.23-0.26) and Am_1 core (Si = 7.6-7.8 a.p.f.u.), at T=620-650°C, and peak pressures of 1.9-2.1 GPa.

Since the chemical domain involved in the Cpx_2+ Pl_1 symplectite formation is likely larger than the microstructural site actually occupied by the symplectite (cf. § 5.2), the symplectitic stage M2 has been modelled using the P-T pseudosection of Fig. 10, calculated for the whole bulk composition. The symplectite-forming reaction (1) previously discussed implies the entry of plagioclase and the coexistence of the Pl_1–Cpx_2 couple, that is modelled by the Cpx+Bt+Am+Pl ±Grt±Rt±Ilm tri- and quadri-variant fields located at T>700°C and 0.4<P<1.1 GPa (Fig. 10). More precise P-T conditions are obtained by comparing the modelled X_{Na}(Cpx) (Fig. 11a) and X_{Ca}(Pl) isopleths with the measured compositions of Cpx_2 (X_{Na}=0.06-0.08) and Pl_1 (X_{Ca}<0.4), constraining the M2 symplectite stage at T=760-800°C, P=0.9-1.0 GPa.

The topology of the pseudosection does not change for a_{H2O} = 0.5. The main consequence of a decrease in water activity is a general shift of all the field boundaries towards lower temperatures (about 50°C down-T for a_{H2O} = 0.5). Therefore, the pseudosection and related isopleths calculated for a_{H2O} = 0.5 will not be discussed in detail (they are available in Fig. 1A and 2A of supplementary material).

6.2. Modelling of the corona stage M3

The M3 stage was characterized by the development of plagioclase ± amphibole ± ilmenite coronas around garnet through reaction (2), which operated in a local microdomain. Therefore, the bulk composition of the whole-rock sample is not representative of the chemical system in which the coronitic texture formed. The bulk composition of the effectively reacting microdomain has been calculated combining the mineral compositions of sample PO2 (Table 1) with the stoichiometric coefficients of reaction (2) (see Groppo et al., 2007 and Cruciani et al., 2008 for a description of the method). This effective bulk composition (SiO_2=45.68, TiO_2=8.40, Al_2O_3=18.14, MgO=4.87, FeO=11.01; CaO=8.51; Na_2O=2.98 wt%) has been used for calculating a second pseudosection in the NCFMASTH system at a_{H2O} = 1.0 (Fig. 12). Potassium was not considered because K-bearing phases are not involved in the coronitic reaction (2). The coronitic assemblage M3, consisting of Pl_2+$Am_{2,3}$+Ilm (Fig. 9) is modelled by the narrow Am+Pl+Grt+Qtz+Rt+Ilm tri-variant field (with Grt <10 vol%) at T<750°C and P=0.7-0.8 GPa. Comparison of the measured and modelled Pl_2 and $Am_{2,3}$ compositions [X_{Ca}(Pl)=0.47-0.51 ; Si(Am)=6.5-6.8 a.p.f.u.; Figs. 13a, b] restricts the P-T conditions of the corona formation to T=610-670°C and P~0.7 GPa (Fig. 12).

7. Discussion

7.1 P-T evolution of the Punta Orvili metabasite and comparison with other Sardinian eclogites

Results from reaction modelling and pseudosection analysis suggest that the Punta Orvili metabasite followed a clockwise P-T path consisting of three main stages (Fig. 14; M1c, M1r, M2 stages reported at H_2O=0.5 for comparison with Giacomini et al., 2005a).

The first portion of this trajectory documents a prograde increase in P and T up to peak-P conditions of about 2.0 GPa at ca. 600°C (amphibole-eclogite facies according to Liou et al., 1998) (Fig. 14a). The Punta Orvili rocks then underwent heating during decompression: temperature peak was reached at about 720°C, 0.9-1.0 GPa (Fig. 14a), corresponding to granulite-facies conditions. During this stage, Cpx_2-Pl_1 symplectites resulted from the breakdown of Cpx_1 according to complex reactions likely involving also Am_1 as a reactant. The modelled reaction (1) is a plausible end member of this set of symplectite-forming reactions. Both microstructural observations and thermodynamic modeling suggest that orthopyroxene did not form during this stage. The subsequent T decrease led to the formation of coronitic assemblages around garnet through reaction (2), under amphibolite-facies P-T conditions (M3 stage). The final exhumation was accompanied by cooling down to greenschist–facies P-T conditions of about 300-400°C and 0.2-0.3 GPa.

The metamorphic evolution preserved by the Punta Orvili metabasite has significant analogies with the well known retrogressed eclogites from Golfo Aranci in NE Sardinia, described by Giacomini et al. (2005a, Fig. 12a) and with other eclogites from the Migmatite Complex, as summarized by Franceschelli et al. (2007). Since for the Golfo Aranci eclogite both the radiometric age of the igneous protolith and the P-T path are well known (Giacomini et al., 2005), the P-T path determined for the Punta Orvili metabasite has been compared with that of the Golfo Aranci retrogressed eclogite. It is to be noted, however, that the protoliths of the Golfo Aranci eclogite and of the Punta Orvili metabasite are different (i.e. N- to T-MORB affinity vs. alkaline basalt of picritic nature; Giacomini et al., 2005, Cruciani et al., 2010).

In the Golfo Aranci eclogites, Giacomini et al. (2005a) recognized a pre-eclogite stage documented by an andesine + edenite + kyanite relic assemblage at T = 580-605°C and P = 0.5-1.0 GPa, followed by peak metamorphism under eclogite-facies conditions of 550-700°C, 1.4-1.7 GPa. More in detail, the P-T conditions calculated with Average PT mode of Thermocalc for the Grt-Jd_{36}-Zo-Ky-Prg-Qtz eclogite assemblage (at a_{H2O}=0.5) were: T=677°C and P=1.89 GPa. This prograde trajectory coincides roughly with the first portion of the P-T path reconstructed for the Punta Orvili metabasite (Fig. 14a).

After the eclogite stage, the rocks from Golfo Aranci underwent significant re-equilibration firstly under granulite-facies conditions (700-800°C, ~ 1.0 GPa), and then under high-T amphibolite-facies conditions (720-830°C) (Giacomini et al., 2005a, Fig. 12a). This means that, after the eclogite stage, both the Punta Orvili metabasite and the Golfo Aranci retrogressed eclogite underwent heating during decompression, reaching approximately the same peak T conditions (Fig. 14).

A medium-T amphibolite event has been described for the Golfo Aranci eclogites at about 550-650°C and 0.6 GPa, at slightly lower pressures than the M3 corona stage constrained for the Punta Orvili metabasite. After this amphibolite event, the Golfo Aranci and Punta Orvili rocks followed the same evolution in greenshist to sub-greenschist-facies conditions.

7.2 H_2O saturated vs. H_2O under-saturated conditions and the preservation of prograde assemblages

In spite of the high-T re-equilibration experienced by the Punta Orvili metabasite, its prograde assemblage is well preserved. Both microstructural data and thermodynamic modelling, in fact, suggest that most of the mineral phases (i.e. Grt, Cpx_1 and Am_1) grew during the prograde M1c and M1r stages, whereas only symplectitic and coronitic microstructures developed during the following M2 and M3 stages. The preservation of prograde assemblages is a feature common to many other granulite-overprinted eclogites occurring in Variscan terranes (see O'Brien and Rötzler, 2003 for a review) and may be explained in terms of H_2O saturated vs. H_2O under-saturated conditions experienced during the metamorphic evolution of such kind of rocks.

If we admit that the system remained close during the rock evolution (i.e. H_2O did not enter in the system from outside), metamorphic reactions may have operated only if the mineral assemblages were H_2O saturated; on the opposite, if P-T conditions under which the mineral assemblages were H_2O under-saturated were reached, metamorphic reactions ceased to be active and the prograde assemblages would be preserved. These concepts are explained in the paper by Guiraud et al. (2001) and represent the key to understand why the prograde assemblage is preserved in the Punta Orvile metabasite, despite the high-T granulitic re-equilibration occurred during the M2 event.

The H_2O isomodes calculated for the pseudosection of Fig. 10 are reported in Fig. 14b. The intersection between the P-T trajectory and the H_2O isomodes clearly shows that, during the prograde evolution from stage M1c to stage M1r, a significant de-hydration occurred, passing from 2.1 to 1.4 wt% H_2O. This means that the prograde assemblages M1c and M1r were H_2O saturated and, therefore, metamorphic reactions were active along the prograde portion of the P-T path (continuous line in Fig. 14b). At about T = 660°C and P = 1.9 GPa (black circle in Fig. 14b), the P-T trajectory becomes tangential to the H_2O isomodes: this means that during the following heating and decompression the mineral assemblages were H_2O under-saturated (dashed line in Fig. 14b) and metamorphic reactions did not operate. This is consistent with the preservation of the prograde assemblage and with the development of symplectitic and coronitic microstructures which are considered as related to H_2O under-saturated conditions.

7.3 Some constraints on the evolution of Variscan Sardinia

Over the last two decades several geodynamic models have been proposed for the evolution of the Variscan chain of Sardinia. According to Carmignani et al. (1994, 2001) the Sardinian chain was formed by the subduction of the South Armorican Ocean, a branch of the Rheic ocean, followed by the collision between the southern Gondwana and the northern Armorica continental plates. More recently, Rossi et al. (2009), (see also Oggiano et al., 2010) proposed that the opening of the South Armorican Ocean occurred in late Ordovician-Early Silurian by back arc spreading and rifting on the North Gondwana margin. The subduction of the South Armorican Ocean beneath the Armorica plate in Silurian-Devonian time was followed, in late Devonian-Early Carboniferous, by the continental collision of Gondwana with the orogenic wedge-Armorica plate.

According to Giacomini et al. (2006), the metamorphic evolution of Sardinian Variscides can be better understood in the context of the plate tectonics model proposed for the history of the Variscan belt by Stampfli et al. (2002), von Raumer et al. (2003, 2009) and references therein. According to von Raumer et al. (2009, their Figs. 5, 6) Sardinia formed part of the Galatian Terrane, a ribbon-like assemblage of basement blocks, separated from the northern Gondwana margin in Devonian times by the opening of an oceanic basin. This Galatian Terrane collided in late Devonian-Carboniferous with the Hanseatic terranes (Laurussia-derived fragments). The collision was followed by the closure of the Palaeotethys and Rhenohercynian oceans with the consequent amalgamation of Gondwana with Laurussia in Late Carboniferous.

Data acquired in the present study can provide information about the geodynamic scenario during the early stages of Variscan metamorphism in Sardinia. In particular, the modelled M1 stage suggests that the prograde evolution of the Punta Orvili metabasite occurred under a geothermal gradient of 10-12°C/km (see Fig. 14), compatible with a relatively hot subduction. Since high thermal gradients are characteristic of slow subduction rates (e.g. Cloos, 1985; Peacock, 1987) and low thermal ones are typical of fast-subducting slabs (e.g. Peacock and Wang, 1999), the relatively shallow, hot gradient of Punta Orvili rocks seems more consistent with the subduction of a small, young marginal basin than with the prolonged subduction of a wider, more thermally mature oceanic plate.

The age of the eclogite-facies metamorphism, which characterises the beginning of the Variscan orogenic cycle in Sardinia, is not well constrained. Zircon U/Pb ages of 400±10 Ma were interpreted by Palmeri et al. (2004) either as the age of the eclogite event in Sardinia or as the result of Pb-loss during the main Variscan event at 327±7Ma. Giacomini et al. (2005b) hypothesized an early Visean age for the eclogite-facies metamorphism.

Exhumation of the Punta Orvili rocks to relatively shallow crustal levels, was accompanied by re-equilibration under granulite- to HT amphibolite-facies conditions, most likely during a period of continental collision (Giacomini et al., 2008). Granulite-facies P-T conditions were probably reached by the eclogites at about 361 – 352 Ma based on the age of the granulite event in the Golfo Aranci eclogite, NE Sardinia (Giacomini et al., 2005a) and the age of the HP (1.8-1.4 GPa) and HT to UHT granulites in the Fautea-Solenzara Unit, southern Corsica (Giacomini et al., 2008). The geothermal gradient in the Punta Orvili metabasite increased up to 20-30°C/km during the decompressional heating from the pre-symplectite M1 stage to the granulitic M2 stage. This geothermal gradient is comparable to the granulite-facies rocks from southern Corsica (20-30°C/km) (Giacomini et al., 2008).

The observed similarities in the P-T conditions of the eclogite-facies suggest that the metabasites from Punta Orvili and Golfo Aranci area shared a common eclogite stage reflecting a common thermal gradient and geodynamic setting in a subduction regime. However, after the eclogite stage sheets or slivers of the amphibolites were stripped off and dragged into two different crustal levels and/or slices, which now correspond to the Low to Medium Grade Metamorphic Complex and the Migmatite Complex.

Recent structural and kinematic studies, carried out in the Medium Grade Metamorphic Complex and High Grade Metamorphic Complex of north-central Sardinia, highlight the presence, after the collisional event and initial vertical extrusion, of a major dextral transpression regime with a top-to-the NW sense of shear followed by activation of a top-to-the SE shear belt (Carosi et al., 2009). During this regime, the eclogite lenses and host rocks were exhumed by post-collisional transpressive processes, whereas extensional tectonics were confined to the closing stages of orogenesis at upper crustal levels.

Acknowledgements

M. Serracino (IGAG-CNR Roma) supported our work with the electron microprobe. We wish to thank Prof. F.M. Elter for his advice and discussion on the structural features of NE Sardinia basement. We are grateful to the reviewers L. Gaggero and C. Wei for their helpful comments and criticism. This work beneficiated from Progetti di Ricerca Locale, Università di Cagliari and MIUR–PRIN 2008 funds to M. Franceschelli is acknowledged.

Appendix A. Supplementary material

Supplementary data associated with this paper can be found, in the online version, at …..

References

Cappelli, B., Carmignani, L., Castorina, F., Di Pisa, A., Oggiano, G., Petrini, R., 1992. A Hercynian suture zone in Sardinia: geological and geochemical evidence. Geodinamica Acta 5, 101–118.

Carmignani, L., Barca, S., Cappelli, B., Di Pisa, A., Gattiglio, M., Oggiano, G., Pertusati, P.C. 1992. A tentative geodynamic model for the Hercynian basement of Sardinia. In: L. Carmignani, F.P. Sassi (Eds). Contributions to the Geology of Italy with special regard to the Paleozoic basements. A volume dedicated to Tommaso Cocozza. IGCP No. 276, Newsletter 5, 61-82.

Carmignani, L., Carosi, R., Di Pisa, A., Gattiglio, M., Musumeci, G., Oggiano, G., Pertusati, P.C., 1994. The Hercynian chain in Sardinia (Italy). Geodinamica Acta 7 (1), 31-47.

Carmignani, L., Oggiano, G., Barca, S., Conti, P., Salvadori, I., Eltrudis, A., Funedda, A., Pasci, S., 2001. Geologia della Sardegna. Note illustrative della Carta Geologica della Sardegna a scala 1:200000. Memorie descrittive della Carta Geologica d'Italia 60, 283 pp.

Carosi, R., Frassi, C., Montomoli, C., 2009. Deformation during exhumation of medium- and high-grade metamorphic rocks in the Variscan chain in northern Sardinia (Italy). Geological Journal 44, 280-305.

Carosi, R., Palmeri, R., 2002. Orogen-parallel tectonic transport in the Variscan belt of northeastern Sardinia (Italy): implications for the exhumation of medium-pressure metamorphic rocks. Geological Magazine 139, 497–511.

Carson, C.J., Powell, R., Clarke, G.L., 1999. Calculated mineral equilibria in CaO-Na_2O-FeO-MgO-Al_2O_3-SiO_2-H_2O: application to the Pouébo Terrane, Pam Peninsula, New Caledonia. Journal of Metamorphic Geology 17, 9-24.

Clarke, G.L., Aitchison, J.C., Cluzel, D., 1997. Eclogites and blueschists of the Pam Peninsula, NE New Caledonia: a reappraisal. Journal of Petrology 38, 843–876.

Cloos, M., 1985. Thermal evolution of convergent plate margins: thermal modeling and re-evaluation of isotopic Ar-ages for blueschists in the Franciscan Complex of California. Tectonics 4, 421–433.

Connolly, J.A.D., 1990. Multivariable phase diagrams: an algorithm based on generalized thermodynamics: American Journal of Science 290, 666-718.

Connolly, J.A.D., 2009. The geodynamic equation of state: what and how. Geochemistry, Geophysics, Geosystems 10, Q10014.

Cortesogno, L., Gaggero, L., Oggiano, G., Paquette, J.L., 2004. Different tectono-thermal evolutionary paths in eclogitic rocks from the axial zone of the Variscan chain in Sardinia (Italy) compared with the Ligurian Alps. Ofioliti 29, 125–144.

Cruciani, G., Dini, A., Franceschelli, M., Puxeddu, M., Utzeri, D., 2010. Metabasite from Variscan NE Sardinia, Italy: within plate OIB-like melts with very high Sr and very low Nd isotopic ratios. European Journal of Mineralogy, 22, 509-523.

Cruciani, G., Elter, F.M., Franceschelli, M., Utzeri, D., Corsi, B., Mallus, G.L., 2007. Mylonitic gneiss in the Variscan basement at Punta Orvili, NE Sardinia, Italy. HT Shear Zones in the Lithosphere, Chiavari (GE), 23-24 maggio 2007. Ofioliti 32 (1), 62-63.

Cruciani, G., Franceschelli, M., Groppo, C., Brogioni, N., Vaselli, O., 2008. Formation of clinopyroxene + spinel symplectites in coronitic gabbros from the Sierra de San Luis (Argentina): a key to post-magmatic evolution. Journal of Metamorphic Geology 26, 759-774.

Dale, J., Powell, R., White, R.W., Elmer, F.L., Holland, J.B., 2005. A thermodynamic model for Ca–Na clinoamphiboles in Na_2O–CaO–FeO–MgO–Al_2O_3–SiO_2–H_2O–O for petrological calculations. Journal of Metamorphic Geology 23, 771–791.

Droop, G.T.R., 1987. A general equation for estimating Fe^{3+} concentration in ferromagnesian silicates and oxides from microprobe analyses, using stoichimetric criteria. Mineralogical Magazine 51, 431-435.

Elter, F.M., 1987. La fascia blastomilonitica tardo-ercinica della valle del Posada nella zona assiale della catena ercinica della Sardegna. PhD Thesis, Università di Siena, 122 p.

Elter, F.M., Franceschelli, M., Ghezzo, C., Memmi, I., Ricci, C.A., 1986. The geology of northern Sardinia. In: Carmignani, L., Cocozza, T., Ghezzo, C., Pertusati, P.C., Ricci, C.A. (Eds.), Guide-Book to the Excursion on the Paleozoic Basement of Sardinia. IGCP Project. Newsletter, vol. 5, pp. 87–102. special issue.

Elter, F.M., Padovano, M., Kraus, R.K., 2010. The emplacement of Variscan HT metamorphic rocks linked to the interaction between Gondwana and Laurussia: structural constraints in NE Sardinia (Italy). Terra Nova 22 (5), 369–377.

Elvevold, S., Gilotti, J.A., 2000. Pressure-temperature evolution of retrogressed kyanite eclogites, Weinschenk Island, North-East Greenland Caledonides. Lithos 53, 127–147.

Endo, S., Wallis, S., Hirata, T., Anczkiewicz, R., Platt, J., Thirlwall, M., Asahara, Y., 2009. Age and early metamorphic history of the Sanbagawa belt: Lu-Hf and P-T constraints from the Western Iratsu eclogite. Journal of Metamorphic Geology 27, 371-384.

Evans, T.P., 2004. A method for calculating effective bulk composition modification due to crystal fractionation in garnet-bearing schist: implication for isopleth thermobarometry. Journal of Metamorphic Geology 22, 547–557.

Faryad, S.W., Nahodilová, R., Dolejš, D., 2010. Incipient eclogite facies metamorphism in the Moldanubian granulites revealed by mineral inclusions in garnet. Lithos 114, 54-69.

Fettes, D., Desmons, J., 2007. Metamorphic rocks – A classification and glossary of terms. Cambridge University Press. 244 pp.

Franceschelli, M., Eltrudis, A., Memmi, I., Palmeri, R., Carcangiu, G., 1998. Multi-stage metamorphic re-equilibration in eclogitic rocks from the Hercynian basement of NE Sardinia (Italy). Mineralogy and Petrology 62, 167–193.

Franceschelli, M., Puxeddu, M., Cruciani, G., 2005. Variscan metamorphism in Sardinia, Italy: review and discussion. In: Carosi R., Dias R., Iacopini D., Rosenbaum G. (eds). The southern Variscan belt. Journal of the Virtual Explorer vol. 19, Paper 2.

Franceschelli, M., Puxeddu, M., Cruciani, G., Utzeri, D., 2007. Metabasites with eclogite facies relics from Variscides in Sardinia, Italy: a review. International Journal of Earth Sciences 96, 795-815.

Gaidies, F., Abart, R., De Capitani, C., Schuster, R., Connolly, J.A.D., Reusser, E. 2006. Characterization of polymetamorphism in the Austroalpine basement east of the Tauern Window using garnet isopleth thermobarometry. Journal of Metamorphic Geology 24, 451–475.

Giacomini, F., Bomparola, R.M., Ghezzo, C., 2005a. Petrology and geochronology of metabasites with eclogite facies relics from NE Sardinia: constraints for the Palaeozoic evolution of Southern Europe. Lithos 82, 221–248.

Giacomini, F., Bomparola, R.M., Ghezzo, C., Guldbransen, H., 2006. The geodynamic evolution of Southern European Variscides: constraint from the U/Pb geochronology and geochemistry of the lower Paleozoic magmatic-sedimentary sequences of Sardinia (Italy). Contribution to Mineralogy and Petrology 152, 19-42.

Giacomini, F., Dallai, L., Carminati, E., Tiepolo, M., Ghezzo, C., 2008. Exhumation of a Variscan orogenic complex: insights into the composite granulitic-amphibolitic metamorphic basement of Southeast Corsica (France). Journal of Metamorphic Geology 26, 403-436.

Giacomini, F., Tiepolo, M., Tribuzio, R., 2005b. 10 micron excimer laser ablation U/Pb geochronology on zircons from kyanite- and zoisite-bearing eclogites of Sardinia and Liguria: new constraints to the variscan Orogeny. FIST, Federazione Italiana di Scienze della Terra, Epitome Geoitalia 2005, Quinto Forum Italiano di Scienze della Terra. Spoleto, 21– 23 settembre 2005.

Godard, G., Martin, S., 2000. Petrogenesis of kelyphites in garnet peridotites: a case study from the Ulten zone, Italian Alps. Journal of Geodynamics 30, 117-145.

Green, E.C.R., Holland, T.J.B., Powell, R., 2007. An order-disorder model for omphacitic pyroxenes in the system jadeite-diopside-hedenbergite-acmite, with applications to eclogitic rocks. American Mineralogist 92, 1181-1189.

Groppo, C., Beltrando, M., Compagnoni, R., 2009. The P–T path of the ultra-high pressure Lago Di Cignana and adjoining high-pressure meta-ophiolitic units: insights into the evolution of the subducting Tethyan slab. Journal of Metamorphic Geology 27, 207-231.

Groppo, C., Lombardo, B., Castelli, D., Compagnoni, R., 2007. Exhumation history of the UHPM Brossasco-Isasca Unit, Dora-Maira Massif, as inferred from a phengite-amphibole eclogite. International Geology Review 49, 142-168.

Groppo, C., Rolfo, F., 2008. P-T evolution of the Aghil Range between Kunlun and Karakorum (SW Sinkiang, China). Lithos 105, 365–378.

Guiraud, M., Powell, R., Rebay, G., 2001. H_2O in metamorphism and unexpected behaviour in the preservation of metamorphic mineral assemblages. Journal of Metamorphic Geology 19, 445-454.

Helbing, H., Frisch, W., Bons, P.D., 2006. South Variscan terrane accretion: Sardinian constraints on the intra- Alpine Variscides. Journal of Structural Geology 28, 1277–1291.

Helgeson, H.C., Delaney, J.M., Nesbitt, H.W., Bird, D.K., 1978. Summary and critique of the thermodynamic properties of rock-forming minerals. American Journal of Sciences 278A, 229 pp.

Holland, T., Baker, J., Powell, R., 1998. Mixing properties and activity-composition relationships of chlorites in the system MgO-FeO-Al_2O_3-SiO_2-H_2O. European Journal of Mineralogy 10, 395-406.

Holland, T.J.B., Powell, R., 1996. Thermodynamics of order-disorder in minerals, 2. Symmetric formalism applied to solid solutions. American Mineralogist 81, 1425–1437.

Holland, T.J.B., Powell, R., 1998. An internally consistent thermodynamic data set for phases of petrologic interest. Journal of Metamorphic Geology 16, 309-343.

Leake, B.E., Woolley, A.R., Arps, C.E.S., Birch, W.D., Gilbert, M.C., Grice, J.D., Hawthorne, F.C., Kato, A., Kisch, H.J., Krivivichev, V.G., Linthout, K., Laird, J., Mandarino, J.A., Maresch, W.V., Nickel, E.H., Rock, N.M.S., Schumacher, J.C., Smith, D.C., Stephenson, N.C.N., Ungaretti, L., Whittaker, E., Youzhi, G., 1997. Nomenclature of amphiboles: report of the subcommittee on amphiboles of the International Mineralogical Association, commission on new minerals and mineral names. Canadian Mineralogist 35, 219-246.

Liou, J.G., Zhang, R.Y., Ernst, W.G., Rumble III, D., Maruyama, S., 1998. High-pressure minerals from deeply subducted metamorphic rocks. In: Hemley, R.J. (Ed.), Ultrahigh-Pressure Mineralogy: Reviews in Mineralogy vol. 37, pp. 33–96. 671 pp.

Marmo, B.A., Clarke, G.L., Powell, R., 2002. Fractionation of bulk rock composition due to porphyroblast growth; effects on eclogite facies mineral equilibria, Pam Peninsula, New Caledonia. Journal of Metamorphic Geology 20, 151–165.

Medaris, G.J., Ducea, M., Ghent, E., Iancu, V., 2003. Conditions and timing of high-pressure Variscan metamorphism in the South Carpathians, Romania. Lithos 70, 141-161.

Messiga, B., Tribuzio, R., Caucia, F., 1991. Amphibole evolution in Variscan eclogite-amphibolites from the Savona crystalline massif (Western Ligurian Alps, Italy): controls on the decompressional P-T-t path. Lithos 27, 215-230.

Miller, C., Sassi, F.P., Armari, G., 1976. On the occurrence of altered eclogitic rocks in north-eastern Sardinia and their implication. Neues Jahrbuch für Geologie und Paläontologie Monatshefte 11, 683–689.

Mogessie, A., Ettinger, K., Leake, B.E., 2004. AMPH-IMA04 a revised Hypercard program to determine the name of an amphibole from chemical analyses according to the 2004 International Mineralogical Association scheme. Mineralogical Magazine 68(5), 825-830.

Möller, C., 1998. Decompressed eclogites in the Sveconorwegian (-Grenvillian) orogen of SW Sweden: petrology and tectonic implications. Journal of Metamorphic Geology 16, 641-656.

Möller, C., 1999. Sapphirine in SW Sweden: a record of Sveconorwegian (-Grenvillian) late-orogenic tectonic exhumation. Journal of Metamorphic Geology 17, 127-141.

Morimoto, M., 1988. Nomenclature of pyroxenes. Mineralogical Magazine 52, 535-550.

O'Brien, P., 1997. Garnet zoning and reaction textures in overprinted eclogites, Bohemian Massif, European Variscides: a record of their thermal history during exhumation. Lithos 41, 119-133.

O'Brien, P.J., Rotzler, J., 2003. High-pressure granulites: formation, recovery of peak conditions and implications for tectonics. Journal of Metamorphic Geology 21, 3–20.

O'Brien, P.J., Vràna, S., 1995. Eclogites with a short-lived granulite facies overprint in the Moldanubian Zone, Czech Republic: petrology, geochemistry and diffusion modelling of garnet zoning. Geologische Rundschau 84, 473–488.

Oggiano, G., Gaggero, L., Funedda, A., Buzzi, L., Tiepolo, M., 2010. Multiple early Paleozoic volcanic events at the northern Gondwana margin: U-Pb age evidence from the Southern Variscan branch (Sardinia, Italy). Gondwana Research 17, 44-58.

Page, F.Z., Essene, E.J., Mukasa, S.B., 2003. Prograde and retrograde history of eclogites from the Eastern Blue Ridge, North Carolina, USA. Journal of Metamorphic Geology 21, 685–698.

Palmeri, R., Fanning, M., Franceschelli, M., Memmi, I., Ricci, C.A., 2004. SHRIMP dating of zircons in eclogite from the Variscan basement in north-eastern Sardinia (Italy). Neues Jahrbuch für Mineralogie Monatshefte 6, 275–288.

Peacock, S.M., 1987. Creation and preservation of subduction related inverted metamorphic gradients. Journal of Geophysical Research, B, Solid Earth and Planets 92, 12,763–12,781.

Peacock, S.M., Wang, K., 1999. Seismic consequences of warm versus cool subduction zone metamorphism: examples from northeast and southwest Japan. Science 286, 937-939.

Pognante, U., Compagnoni, R., Gosso, G., 1980. Micromesostructural relationships in the continental eclogitic rocks of the Sesia-Lanzo zone: a record of a subduction cycle (Italian Western Alps). Rendiconti della Società Italiana di Mineralogia e Petrologia 36, 169-186.

Powell, R., Holland, T.J.B., 2008. On thermobarometry. Journal of Metamorphic Geology 26, 155–179.

Rossi, P., Oggiano, G., Cocherire, A., 2009. A restored section of the “southern Variscan realm” accross the Corsica-Sardinia microcontinent. C.R. Geoscience 341, 224-238.

Stampfli, G.M., von Raumer, J.F., Borel, G.D., 2002. Paleozoic evolution of pre-Variscan terranes: from Gondwana to the Variscan collision. Geological Society of America Special Paper 364, 263-280.

Štîpská, P., Pitra P., Powell, R., 2006. Separate or shared metamorphic histories of eclogites and surrounding rocks? An example from the Bohemian Massif. Journal of Metamorphic Geology 24, 219-240.

Štîpská,, P., Powell, R., 2005. Constraining the P-T path of a MORB-type eclogite using pseudosections, garnet zoning and garnet-clinopyroxene thermometry: an example from the Bohemian Massif. Journal of Metamorphic Geology 23, 725–743.

Stüwe, K., 1997. Effective bulk composition changes due to cooling: a model predicting complexities in retrograde reaction textures. Contributions to Mineralogy and Petrology 129, 43–52.

von Raumer, J.F., Bussy, F., Stampfli, G.M., 2009. The Variscan evolution in the External massifs of the Alps and place in their Variscan framework. C.R. Geoscience 341, 239-252.

von Raumer, J.F., Stampfli, G.M., Bussy, F., 2003. Gondwana- derived microcontinents -the constituents of the Variscan and Alpine collisional orogens. Tectonophysics 365, 7-22.

Wei, C.J., Powell, R., Zhang, L.F., 2003. Eclogite from the southern Tianshan, NW China: petrological characteristic and calculated mineral equilibria in the Na_2O-CaO-FeO-MgO- Al_2O_3-SiO_2- H_2O system. Journal of Metamorphic Geology 21, 163–179.

Wei, C.J., Yang, Y., Su, L., Song, S.G., Zhang, L.F., 2009. Metamorphic evolution of low-T eclogite from the North Qilian orogen, NW China: evidence from petrology and calculated phase equilibria in the system NCKFMASHO. Journal of Metamorphic Geology 27, 55–70.

White, R.W., Powell, R., Holland, T.J.B., 2007. Progress relating to calculation of partial melting equilibria for metapelites. Journal of Metamorphic Geology 25, 511–527.

Zuluaga, C.A., Stowell, H., Tinkham, D., 2005. The effect of zoned garnet on metapelite pseudosection topology and calculated metamorphic P-T paths. American Mineralogist 90, 1619–1628.

Figure captions

Fig. 1. Geological sketch map from Punta Orvili to Golfo Aranci area, NE Sardinia. In the upper-right corner the tectono-metamorphic zoning of the Variscan chain of Sardinia PAL: Posada-Asinara Line. Modified from Carmignani et al. (2001).

Fig. 2. Photomicrographs showing the relevant microstructures of sample PO2. (a) Garnet with amphibole (Am_1) inclusions surrounded by amphibole, biotite, medium-grained pyroxene (Cpx_1) and clinopyroxene + plagioclase symplectite (Cpx_2 + Pl_1). Cross Polarized Light (XPL). (b) Detail of clinopyroxene + plagioclase symplectite. XPL. (c) Cpx_1 relic showing equilibrium contacts with Am_1 (triple joints, see asterisks). Plane Polarized Lght (PPL). (d) Cpx_1 + Pl_1 symplectite growing at the expenses of Cpx_1. Am_1 is likely involved in the symplectite forming reaction. PPL. (e, f) Garnet crystal with fine-grained Am_1 inclusions, showing equilibrium contacts with larger Am_1 (see asterisk). PPL (e), XPL (f).

Fig. 3. Back Scattered Electron images of the Punta Orvili metabasites. (a) Coronitic garnet surrounded by micrometre-thick corona of plagioclase (Pl_2). Cpx_1 contains small oriented quartz needles. (b) Amphibole (Am_1) characterized by inclusion-rich core surrounded by inclusion-free rim. Interface between Am_1 and garnet is marked by an Al-rich amphibole (Am_2). (c) Relationships between clinopyroxene, Cpx_2 + Pl_1 symplectites and coronitic garnet at the garnet/clinopyroxene interface. Symplectitic minerals and coronitic plagioclase are separated by thin layer of amphibole (Am_2). (d) Coronitic garnet, with Am_1 inclusions, surrounded by a micrometre-thick corona of Pl_2 + Am_3. Coronitic minerals in the upper-right corner of the photograph include plagioclase and ilmenite. (e) Cpx_2 + Pl_1 symplectites formed at the edge of elongated clinopyroxene (Cpx_1) crystal. Note the alignment of rutile inclusions in Am_1 amphibole. (f) Coronitic microstructure consisting of Pl_2 + Am_3 + ilmenite developed on garnet

relict. On the right side, amphibole pseudomorphs on symplectitic clinopyroxene simulate the occurrence of amphibole and plagioclase symplectite.

Fig. 4. Clinopyroxene classification in the Wo-En-Fs and (Wo+En+Fs)-Jd-Ae diagrams (Morimoto, 1988). All textural types of clinopyroxene are diopside, but Cpx_1 granoblastic clinopyroxene is enriched in jadeite component as compared to Cpx_2 symplectitic clinopyroxene.

Fig. 5. Rim-core-rim compositional profile of Na, Ca, Mg, Fe^{2+} along a Cpx_1 crystal of sample PO2. Note progressive increase in Na counterbalanced by Ca decrease from core to rim.

Fig. 6. Rim-core-rim compositional profile along a garnet crystal of sample PO2 showing a progressive decrease in Ca counterbalanced by Fe and Mg increase from core to rim.

Fig. 7. Rim-core-rim compositional profile along an amphibole crystal (Am_1) of sample PO2 showing progressive decrease in Si and increase in Ti, Al, Ca, Na and K from core to rim.

Fig. 8. Amphibole classification according to Leake et al. (1997). Matrix amphibole (Am_1) range in composition from magnesiohornblende to actinolite, whereas Am_1 included in garnet is mainly magnesiohornblende. Amphibole in contact with garnet (Am_2) is magnesiohornblende to tschermakite, whereas coronitic amphibole (Am_3) is mostly magnesiohornblende. Amphibole filling late veins and fractures is actinolite. Additional amphibole analyses not reported in Table 1 are also shown.

Fig. 9. Metamorphic evolution of the metabasite from Punta Orvili, as inferred from microstructural relationships. Cpx_1: granoblastic clinopyroxene; Cpx_2: symplectitic clinopyroxene, Am_1: matrix amphibole and amphibole included in garnet; Am_2: amphibole halo in contact with garnet; Am_3: coronitic amphibole; Pl_1: symplectitic plagioclase; Pl_2: coronitic plagioclase; (c): core; (r): rim.

Fig. 10. P–T pseudosection for sample PO2 in the NCKFMASTH system calculated at aH_2O = 1. White, light-, medium-, dark-, and very dark-grey fields are di-, tri-, quadri-, penta-, and hexa-variant fields, respectively. Dotted ellipses represent P-T conditions for pre-symplectite (M1c and M1r) and symplectite (M2) stages estimated using garnet, clinopyroxene, amphibole and plagioclase compositional isopleths (see Fig. 11).

Fig. 11. Contour lines for P-T pseudosection of Fig. 10 showing variation in : (a) X_{Na} [Na/(Na+Ca)] in clinopyroxene, (b) Si content (a.p.f.u.) in amphibole, (c) X_{Ca} [Ca/(Ca+Mg+Fe)] in garnet, and (d) X_{Mg} [Mg/(Mg+Fe+Ca)] in garnet. X_{Na}, X_{Ca}, X_{Mg} expressed in %. Dotted ellipses constrain P-T conditions for pre-symplectite (M1c and M1r) and symplectite (M2) stages, respectively.

Fig. 12. P–T pseudosection calculated in simplified NCFMASTH system at a_{H2O} = 1.0, using bulk composition of the effectively reacting corona microdomain in sample PO2. This effective bulk composition has been calculated by combining mineral compositions and stoichiometric coefficients of reaction (2). White-, light-, medium-, dark-, and very dark-grey fields are di-, tri-, quadri-, penta-, and hexa-variant fields, respectively. Dotted ellipse represents P-T conditions of corona stage (M3) estimated using garnet, amphibole and plagioclase compositional isopleths (see Fig. 13).

Fig. 13. Contour lines for P-T pseudosection of Fig. 12 showing variation in: (a) anorthite (X_{Ca}) content in plagioclase, (b) Si content (a.p.f.u.) in amphibole, (c) X_{Ca} in garnet, (d) X_{Mg} in garnet. X_{Ca}, X_{Mg} expressed in %. Dotted ellipse constrains P-T conditions for corona stage (M3).

Fig. 14. (a) Comparison of P-T path reconstructed for Punta Orvili metabasite and P-T path of the retrogressed eclogites from Golfo Aranci (Giacomini et al., 2005a). The M1c, M1r, and M2 stages of the Punta Orvili metabasite are recalculated at a_{H2O} = 0.5 for a better comparison with Giacomini et al. (2005a) data. Metamorphic facies from Liou et al. (1998). PR-A= prograde amphibolite; E=eclogite; GR=granulite; HT-Amp=high-temperature amphibolite; MT-Amp=medium-temperature amphibolite. (b)

Contour lines for P-T pseudosections of Fig. 10 (at a_{H2O} =1.0) showing the H_2O wt%. The continuous portion of the P-T trajectory indicates H_2O saturated conditions, whereas the dashed portion indicated H_2O under-saturated conditions. The black circle shows the P-T conditions at which the P-T trajectory becomes tangential to the H_2O isomodes (i.e. the P-T conditions from which the metamorphic assemblage has been preserved) (see Guiraud et al., 2001 for further discussion).

Table captions

Table 1. Selected microprobe analyses and structural formula of amphibole, garnet, clinopyroxene, plagioclase, biotite, ilmenite from sample PO2.

Supplementary material

Fig. 1A. P–T pseudosection for sample PO2 in the NCKFMASTH system calculated at a_{H2O} = 0.5. White, light-, medium-, dark-, and very dark-grey fields are di-, tri-, quadri-, penta-, and hexa-variant fields, respectively. Dotted ellipses represent P-T conditions for pre-symplectite (M1c and M1r) and symplectite (M2) stages estimated using garnet, clinopyroxene, amphibole and plagioclase compositional isopleths (see Fig. 2A).

Fig. 2A. Contour lines for P-T pseudosection of Fig. 1A showing variation in: (a) X_{Na} [Na/(Na+Ca)] in clinopyroxene, (b) Si content (a.p.f.u.) in amphibole, (c) X_{Ca} [Ca/(Ca+Mg+Fe)] in garnet, and (d) X_{Mg} [Mg/(Mg+Fe+Ca)] in garnet. X_{Na}, X_{Ca}, X_{Mg} expressed in %. Dotted ellipses constrain P-T conditions for pre-symplectite (M1c and M1r) and symplectite (M2) stages, respectively.

Table 1A. Selected microprobe analyses and structural formula of amphibole, garnet, clinopyroxene, plagioclase, biotite, ilmenite and titanite from sample U126.

Table 2A. Selected microprobe analyses and structural formula of amphibole, garnet, clinopyroxene, plagioclase, biotite, ilmenite from sample PO6.

Fig. 1

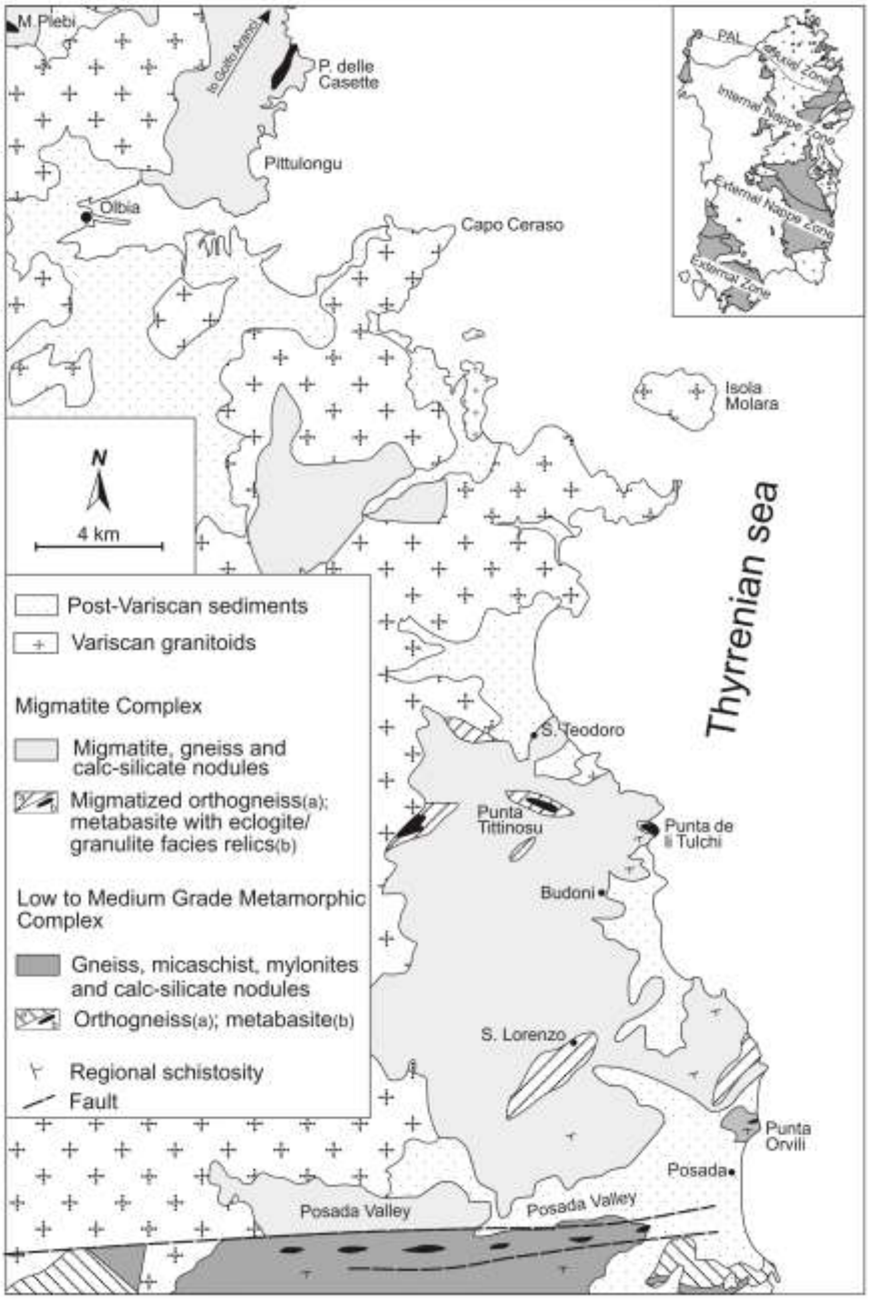
M. Plebi
to Golfo Aranci
P. delle
Casette
Pittulongu
Olbia
Capo Ceraso
PAL
Axial Zone
Internal Nappe Zone
External Nappe Zone
External Zone
Isola
Molara
N
4 km
Thyrrenian sea
Post-Variscan sediments
Variscan granitoids
Migmatite Complex
Migmatite, gneiss and
calc-silicate nodules
Migmatized orthogneiss(a);
metabasite with eclogite/
granulite facies relics(b)
Low to Medium Grade Metamorphic
Complex
Gneiss, micaschist, mylonites
and calc-silicate nodules
Orthogneiss(a); metabasite(b)
Regional schistosity
Fault
S. Teodoro
Punta
Tittinosu
Punta de
li Tulchi
Budoni
S. Lorenzo
Punta
Orvili
Posada
Posada Valley
Posada Valley

Fig. 2

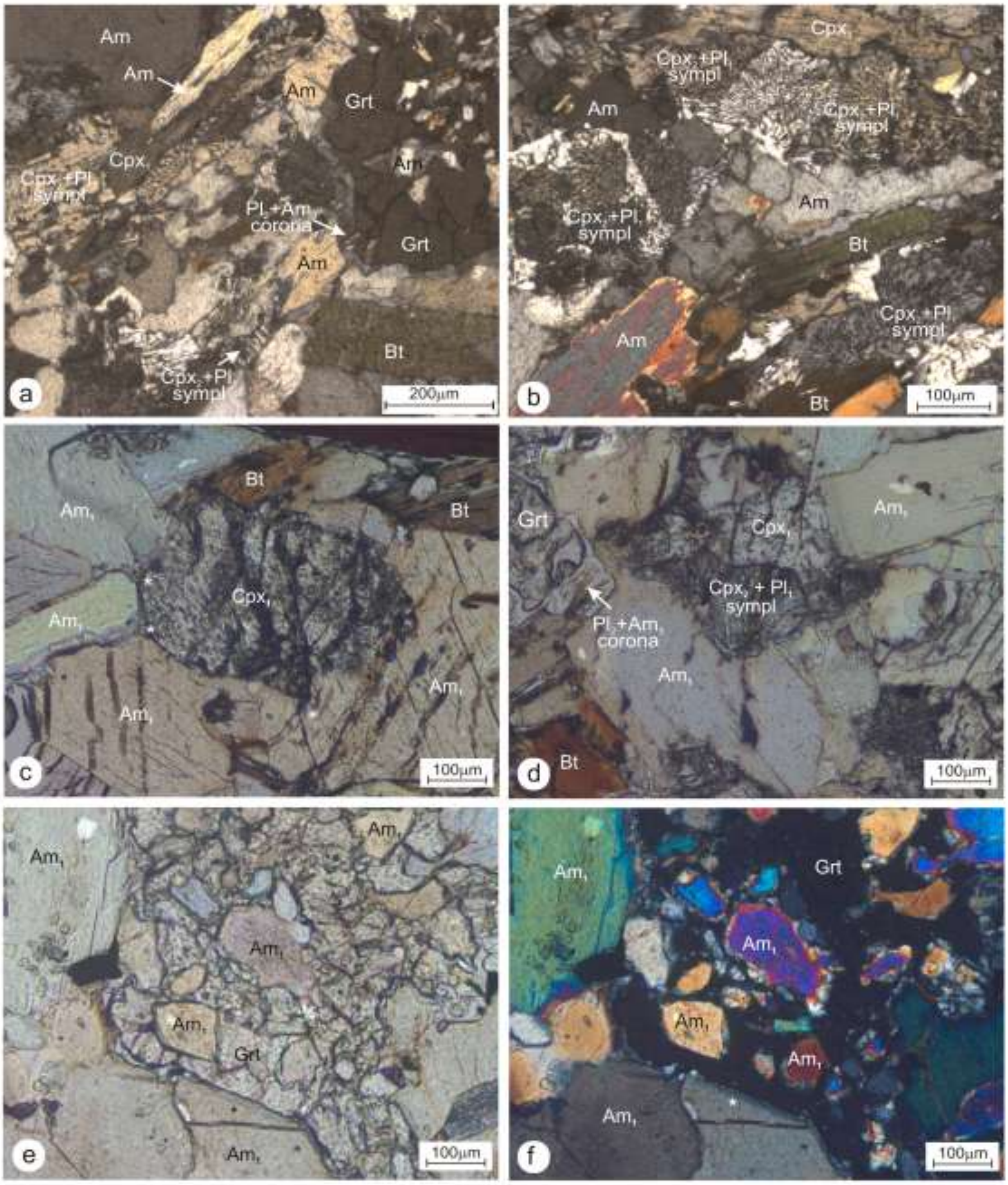

Fig. 3

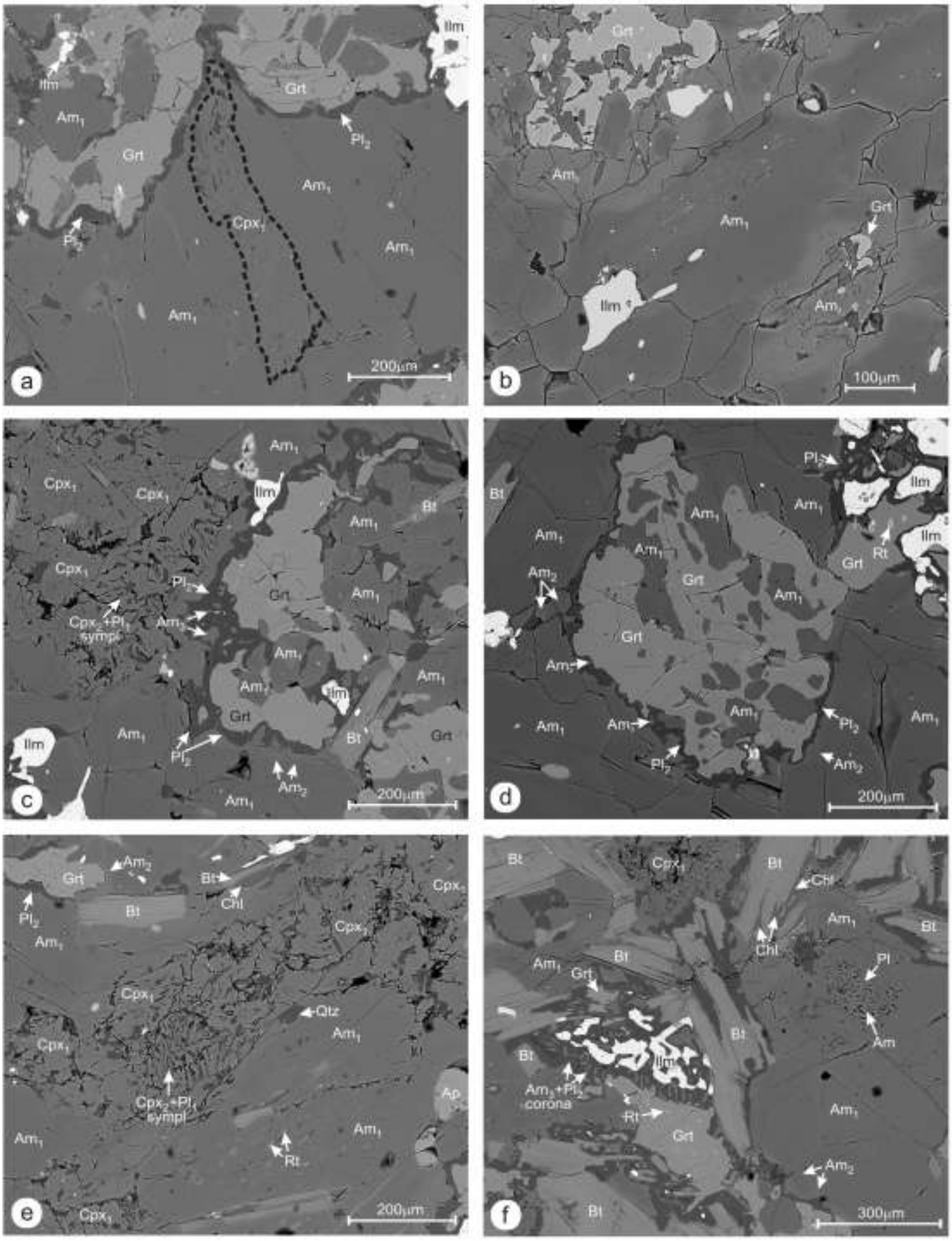

a
Ilm
Am1
Grt
Pl2
Cpx1
200μm
b
Grt
Am1
Ilm
100μm
c
Cpx1
Cpx2+Pl1 sympl
Am1
Ilm
Bt
Pl2
Am2
Grt
200μm
d
Bt
Am1
Am2
Grt
Pl2
Ilm
Rt
200μm
e
Grt
Am2
Bt
Chl
Pl2
Am1
Cpx1
Cpx2+Pl1 sympl
Qtz
Ap
Rt
200μm
f
Bt
Cpx1
Chl
Am1
Pl
Am
Grt
Ilm
Am3+Pl2 corona
Rt
Am2
300μm

Fig. 4

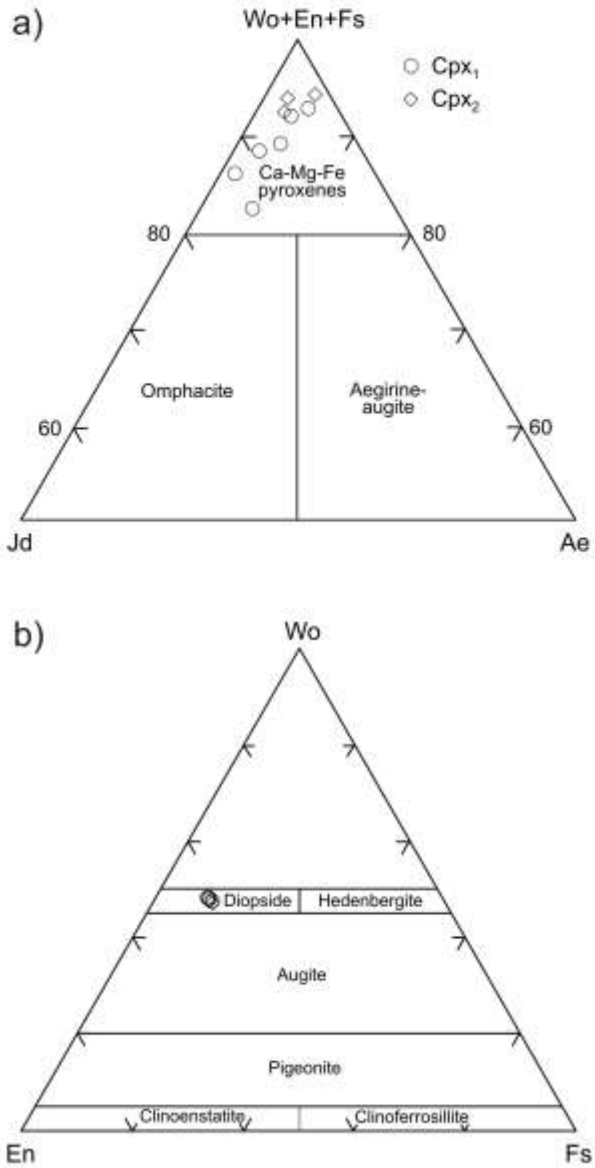
a)
Wo+En+Fs
Cpx1
Cpx2
Ca-Mg-Fe pyroxenes
80
80
Omphacite
Aegirine-augite
60
60
Jd
Ae
b)
Wo
Diopside
Hedenbergite
Augite
Pigeonite
Clinoenstatite
Clinoferrosillite
En
Fs

Fig. 5

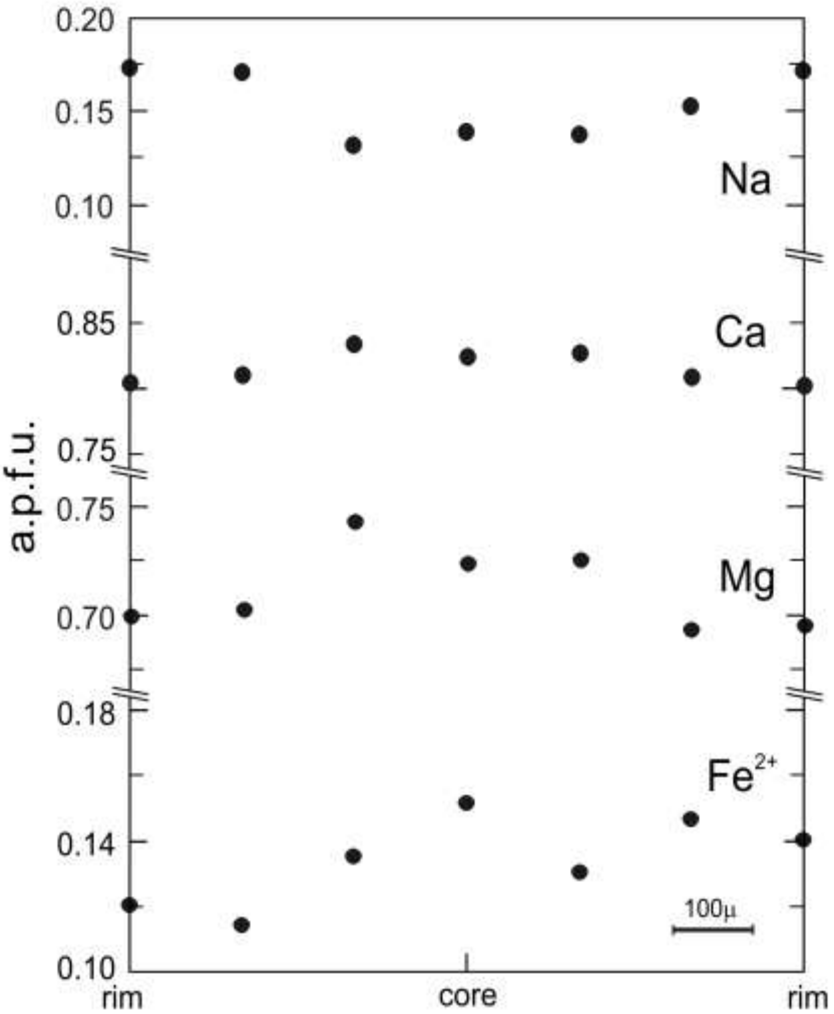

a.p.f.u.
0.20
0.15
0.10
Na
0.85
0.75
Ca
0.75
0.70
Mg
0.18
0.14
0.10
Fe2+
100µ
rim
core
rim

Fig. 6

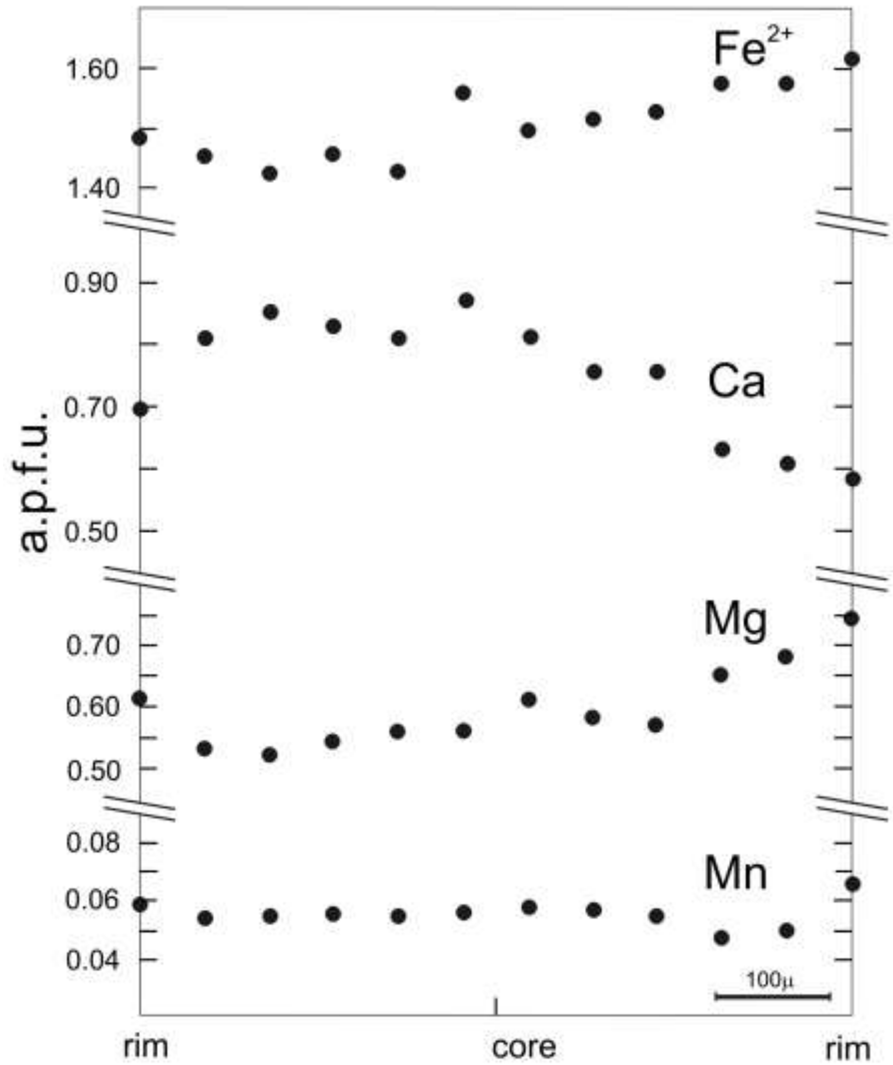

Fe2+
Ca
Mg
Mn
a.p.f.u.
1.60
1.40
0.90
0.70
0.50
0.70
0.60
0.50
0.08
0.06
0.04
100µ
rim
core
rim

Fig. 7

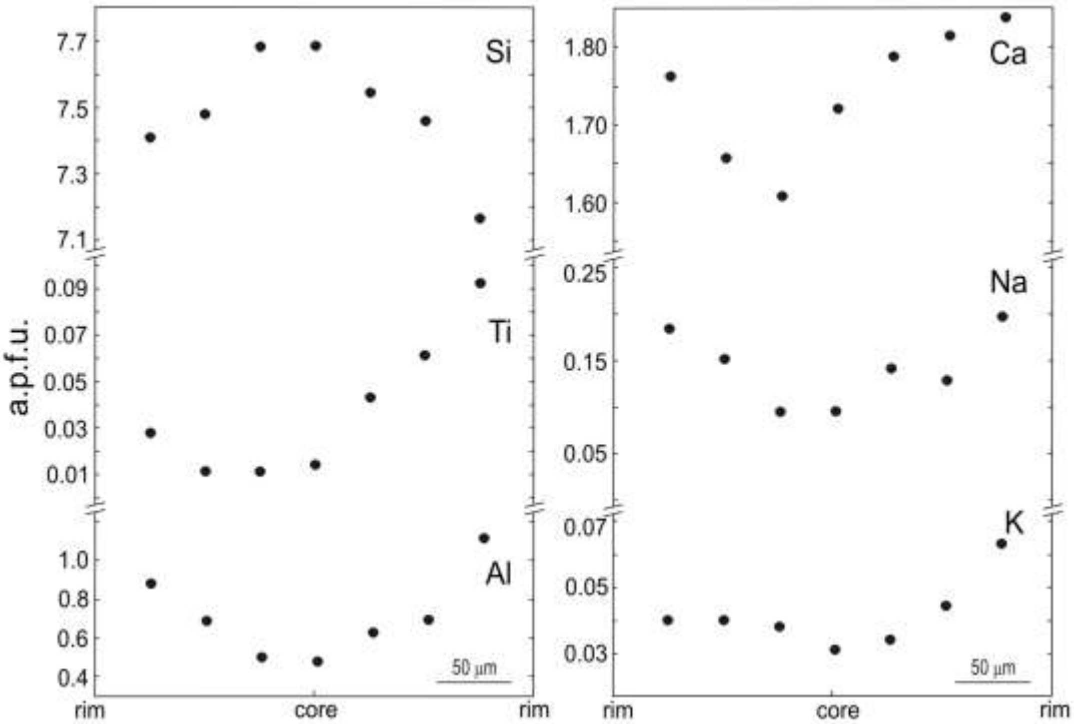

Si
Ti
Al
Ca
Na
K
a.p.f.u.
7.7
7.5
7.3
7.1
0.09
0.07
0.05
0.03
0.01
1.0
0.8
0.6
0.4
1.80
1.70
1.60
0.25
0.15
0.05
0.07
0.05
0.03
50 µm
50 µm
rim
core
rim
rim
core
rim

Fig. 8

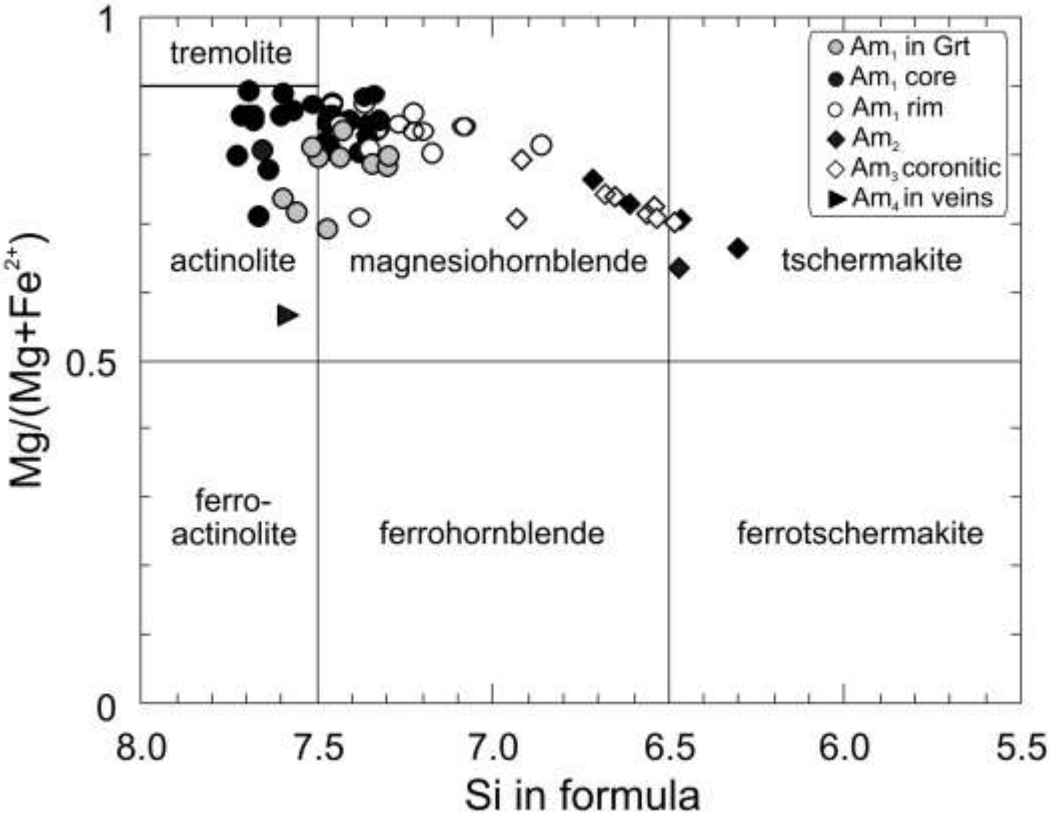

tremolite
actinolite
magnesiohornblende
tschermakite
ferro-
actinolite
ferrohornblende
ferrotschermakite
Am1 in Grt
Am1 core
Am1 rim
Am2
Am3 coronitic
Am4 in veins
Mg/(Mg+Fe2+)
Si in formula
1
0.5
0
8.0
7.5
7.0
6.5
6.0
5.5

Fig. 9

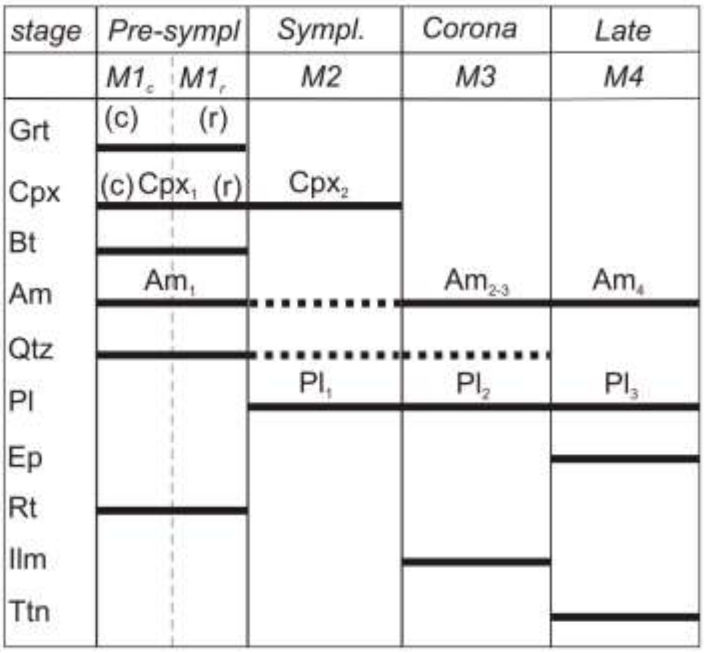
stage
Pre-sympl
Sympl.
Corona
Late
M1c
M1r
M2
M3
M4
Grt
Cpx
Bt
Am
Qtz
Pl
Ep
Rt
Ilm
Ttn
(c)
(r)
(c) Cpx1 (r)
Cpx2
Am1
Am2-3
Am4
Pl1
Pl2
Pl3

Fig. 10

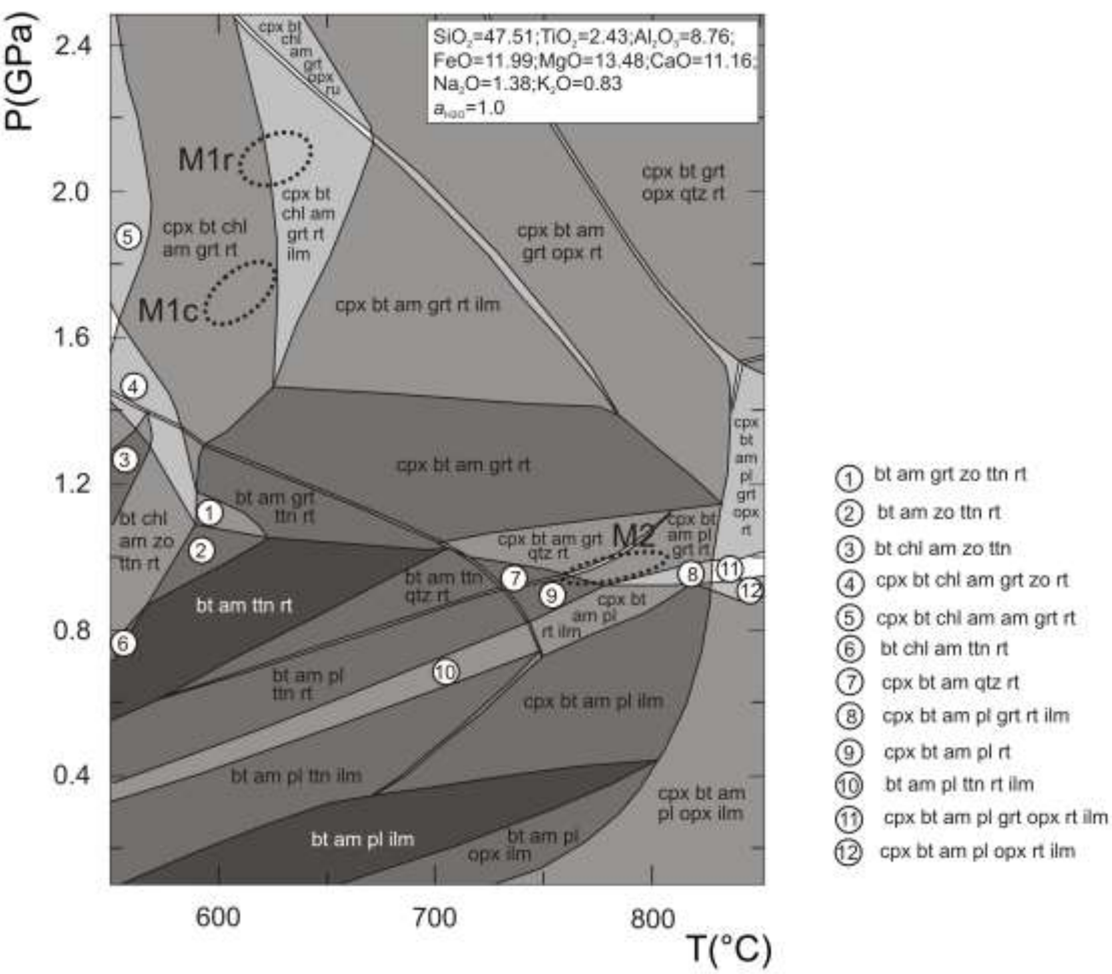

P(GPa)
T(°C)
SiO2=47.51;TiO2=2.43;Al2O3=8.76;
FeO=11.99;MgO=13.48;CaO=11.16;
Na2O=1.38;K2O=0.83
aH2O=1.0
M1r
M1c
M2
cpx bt chl am grt rt
cpx bt chl am grt rt ilm
cpx bt am grt rt ilm
cpx bt am grt opx rt
cpx bt grt opx qtz rt
cpx bt am grt rt
bt am grt ttn rt
bt chl am zo ttn rt
bt am ttn rt
bt am ttn qtz rt
cpx bt am grt qtz rt
cpx bt am pl grt rt
cpx bt am pl rt ilm
bt am pl ttn rt
cpx bt am pl ilm
bt am pl ttn ilm
bt am pl ilm
bt am pl opx ilm
cpx bt am pl opx ilm
1 bt am grt zo ttn rt
2 bt am zo ttn rt
3 bt chl am zo ttn
4 cpx bt chl am grt zo rt
5 cpx bt chl am am grt rt
6 bt chl am ttn rt
7 cpx bt am qtz rt
8 cpx bt am pl grt rt ilm
9 cpx bt am pl rt
10 bt am pl ttn rt ilm
11 cpx bt am pl grt opx rt ilm
12 cpx bt am pl opx rt ilm

Fig. 11

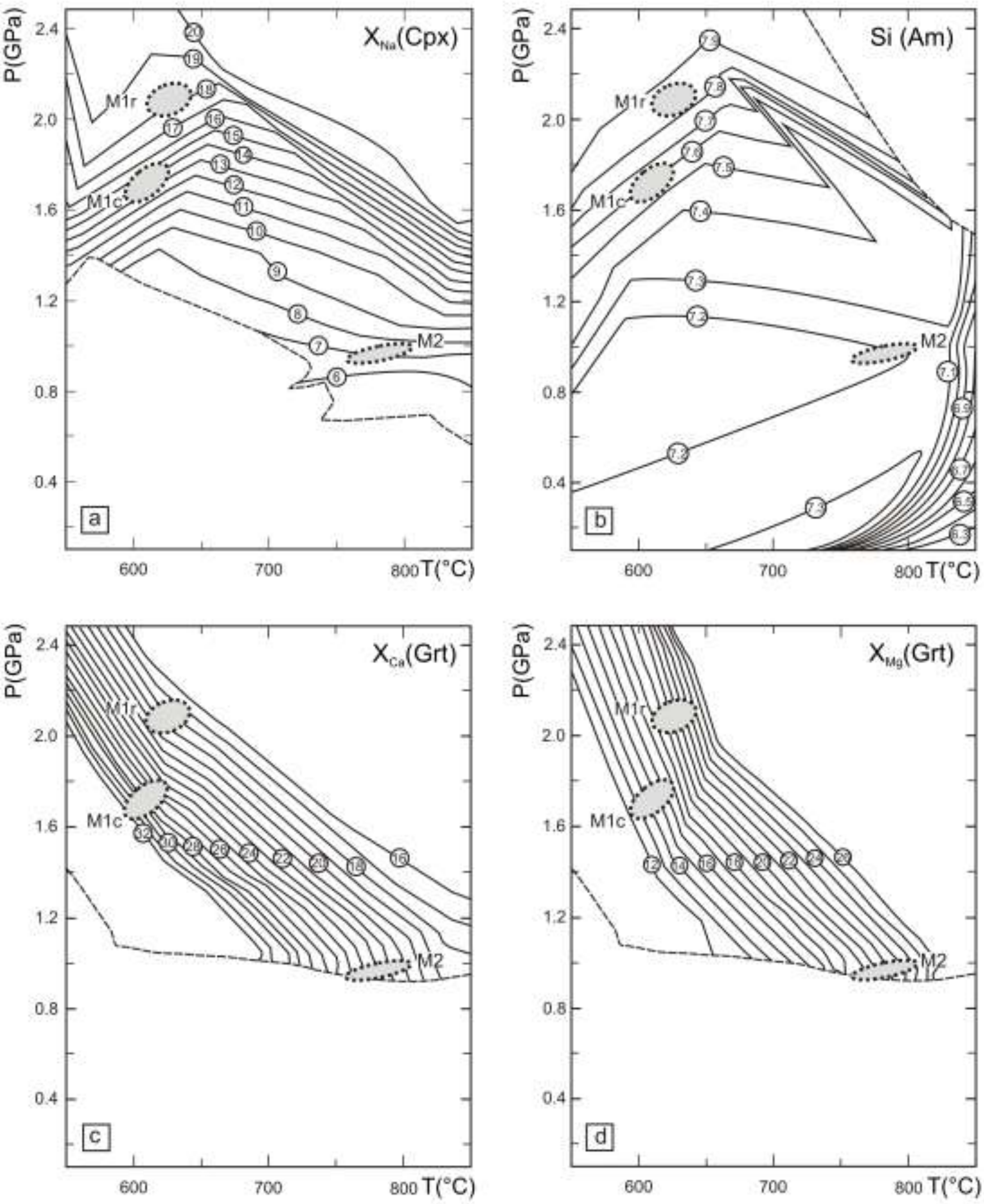

Fig. 12

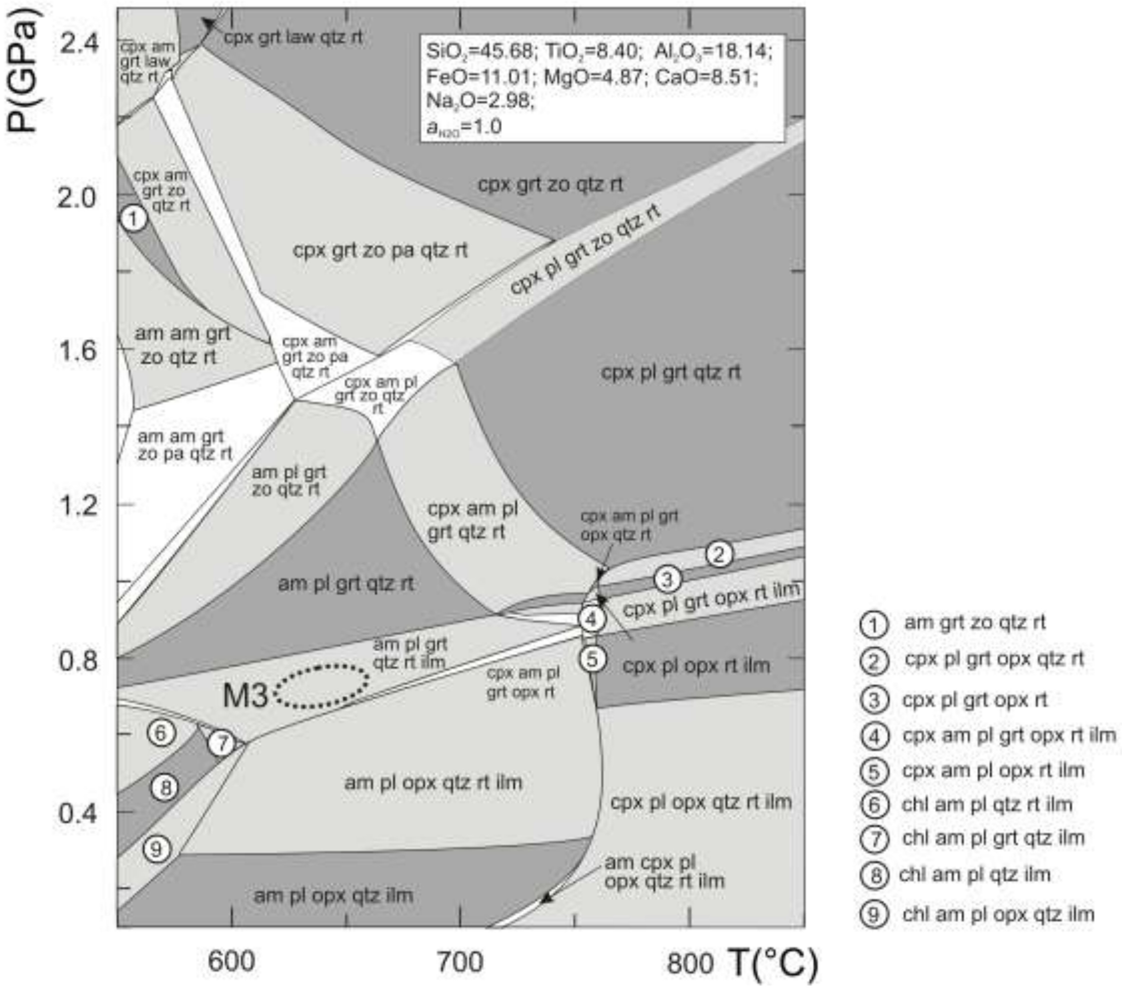

SiO2=45.68; TiO2=8.40; Al2O3=18.14;
FeO=11.01; MgO=4.87; CaO=8.51;
Na2O=2.98;
aH2O=1.0
cpx grt law qtz rt
cpx am grt law qtz rt
cpx am grt zo qtz rt
cpx grt zo qtz rt
cpx grt zo pa qtz rt
cpx pl grt zo qtz rt
am am grt zo qtz rt
cpx am grt zo pa qtz rt
cpx am pl grt zo qtz rt
cpx pl grt qtz rt
am am grt zo pa qtz rt
am pl grt zo qtz rt
cpx am pl grt qtz rt
cpx am pl grt opx qtz rt
am pl grt qtz rt
cpx pl grt opx rt ilm
am pl grt qtz rt ilm
cpx am pl grt opx rt
cpx pl opx rt ilm
M3
am pl opx qtz rt ilm
cpx pl opx qtz rt ilm
am cpx pl opx qtz rt ilm
am pl opx qtz ilm
P(GPa)
2.4
2.0
1.6
1.2
0.8
0.4
600
700
800
T(°C)
1 am grt zo qtz rt
2 cpx pl grt opx qtz rt
3 cpx pl grt opx rt
4 cpx am pl grt opx rt ilm
5 cpx am pl opx rt ilm
6 chl am pl qtz rt ilm
7 chl am pl grt qtz ilm
8 chl am pl qtz ilm
9 chl am pl opx qtz ilm

Fig. 13

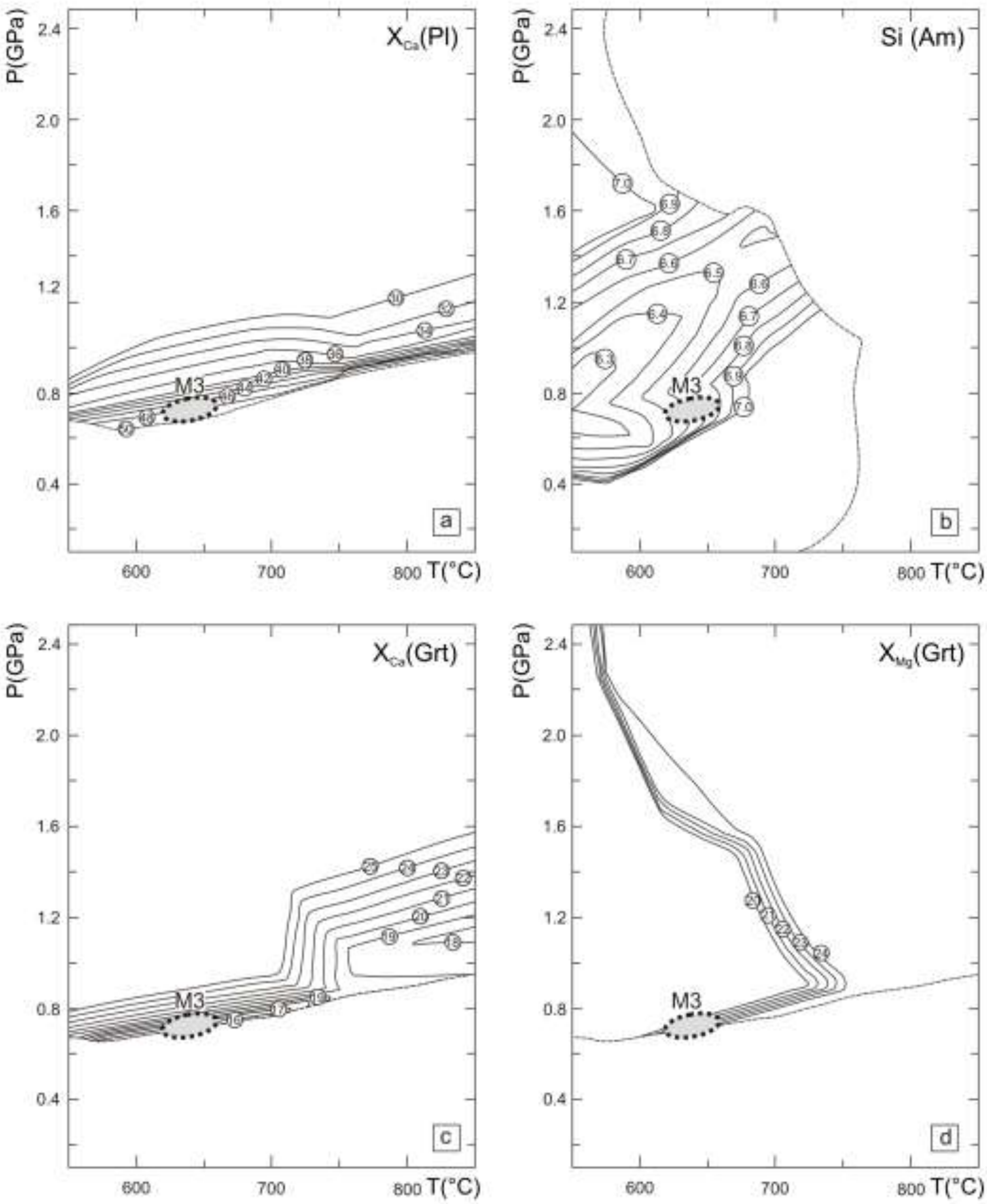

X_Ca(Pl)
Si (Am)
X_Ca(Grt)
X_Mg(Grt)
M3
a
b
c
d
P(GPa)
2.4
2.0
1.6
1.2
0.8
0.4
600
700
800
T(°C)

Fig. 14

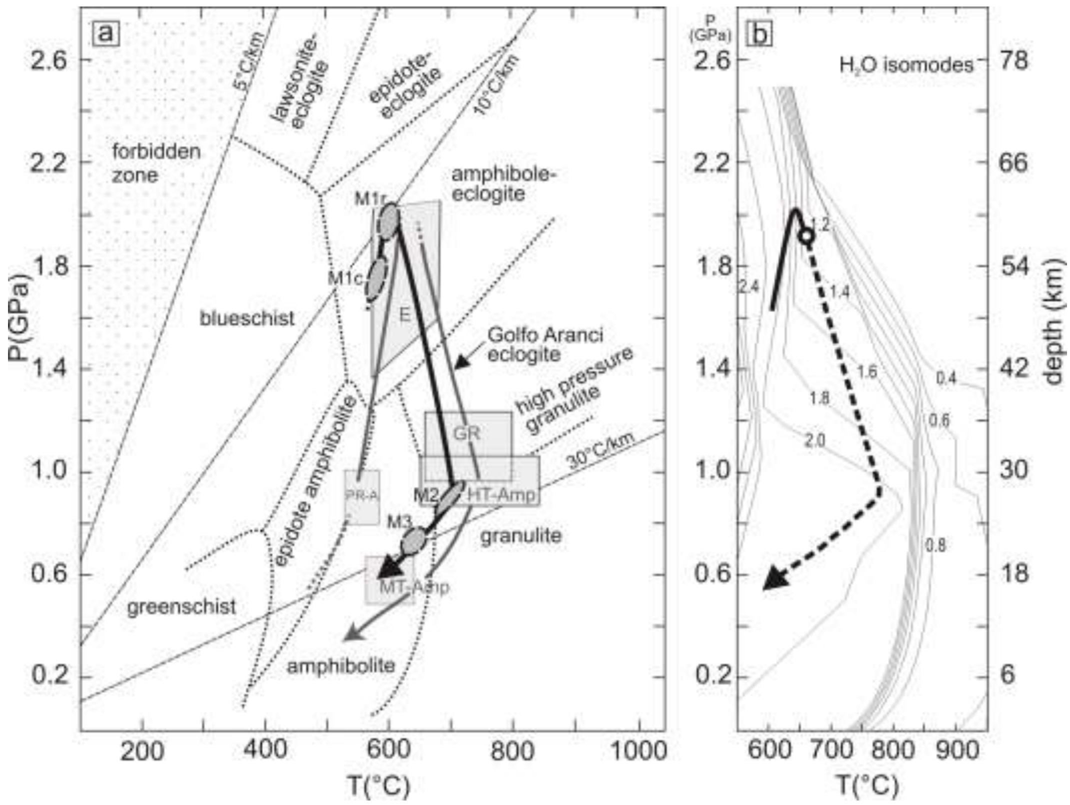
a
forbidden zone
5°C/km
lawsonite-eclogite
epidote-eclogite
10°C/km
amphibole-eclogite
blueschist
M1r
M1c
E
Golfo Aranci eclogite
high pressure granulite
GR
30°C/km
PR-A
M2
HT-Amp
M3
granulite
epidote amphibolite
MT-Amp
greenschist
amphibolite
P(GPa)
T(°C)
b
P (GPa)
H2O isomodes
depth (km)
T(°C)

Table 1

Table 1

	PO2	PO2	PO2	PO2	PO2	PO2	PO2	PO2	PO2	PO2	PO2	PO2	PO2	PO2	PO2
	$Am1_{rim}$	$Am1_{core}$	$Am1_{rim}$	Am_3	Am_3	Am_4	Grt_{core}	Grt_{rim}	$Cpx1_{core}$	$Cpx1_{rim}$	Cpx_2	Pl_1	Pl_2	Bt	Ilm
SiO_2	51.49	53.95	49.31	44.58	45.78	51.62	38.14	37.50	53.79	53.20	53.03	59.91	56.07	35.20	0.01
TiO_2	0.26	0.13	0.84	1.35	0.8	0.01	0.10	0.01	0.05	0.01	0.11	0.03	0.03	4.82	52.49
Al_2O_3	5.16	2.83	6.48	11.98	10.85	5.05	22.23	22.02	3.84	3.99	1.46	23.67	27.42	15.51	-
Cr_2O_3	0.08	0.09	0.08	0.48	0.17	-	0.13	0.10	0.13	0.20	0.21	-	0.03	0.12	0.14
FeO	9.96	9.61	9.66	10.96	11.13	16.64	24.13	24.46	5.58	5.67	6.51	0.41	0.28	14.44	45.34
MnO	0.13	0.08	0.02	0.08	0.06	0.02	0.85	0.98	-	0.03	0.11	0.07	-	0.02	0.79
MgO	17.33	18.56	16.95	13.30	14.07	11.56	4.89	6.35	13.22	12.68	14.61	0.31	-	13.89	0.15
CaO	11.44	11.28	11.81	11.70	11.79	11.57	10.6	6.91	20.90	20.25	22.98	6.11	9.44	-	-
Na_2O	0.66	0.34	0.70	1.32	1.30	0.53	-	-	1.95	2.41	0.77	7.64	5.96	0.23	0.04
K_2O	0.22	0.17	0.34	0.57	0.52	0.32	-	-	-	-	0.02	0.04	0.03	8.10	-
BaO	-	-	-	-	-	-	-	-	-	-	-	-	-	2.54	-
F	0.03	0.06	0.11	0.07	-	-	-	-	-	-	-	-	0.02	0.12	0.10
Total	96.76	97.10	96.30	96.39	96.47	97.32	101.07	98.33	99.46	98.44	99.81	98.19	99.28	94.99	99.06
oxy	23	23	23	23	23	23	12	12	6	6	6	8	8	22	3
Si	7.36	7.66	7.09	6.53	6.68	7.58	2.95	2.95	1.97	1.97	1.96	2.72	2.54	5.36	-
Ti	0.03	0.01	0.09	0.15	0.09	-	0.01	-	-	-	-	-	-	0.55	1.00
Al	0.87	0.47	1.10	2.07	1.87	0.87	2.02	2.04	0.17	0.17	0.07	1.26	1.46	2.78	-
Cr	0.01	0.01	0.01	0.06	0.02	-	0.01	0.01	-	0.01	0.01	-	-	0.01	-
Fe^{2+}	0.88	1.00	0.70	1.12	1.07	2.02	1.51	1.57	0.15	0.12	0.13	0.02	0.01	1.84	0.96
Fe^{3+}	0.31	0.14	0.46	0.23	0.29	0.03	0.05	0.05	0.02	0.06	0.07	-	-	-	-
Mn	0.02	0.01	-	0.01	0.01	-	0.06	0.07	-	-	-	-	-	-	0.02
Mg	3.69	3.93	3.63	2.91	3.06	2.53	0.56	0.75	0.72	0.70	0.80	0.02	-	3.16	0.01
Ca	1.75	1.72	1.82	1.84	1.84	1.82	0.83	0.58	0.82	0.80	0.91	0.30	0.46	-	-
Na	0.18	0.09	0.20	0.38	0.37	0.15	-	-	0.14	0.17	0.06	0.67	0.52	0.07	-
K	0.04	0.03	0.06	0.11	0.10	0.06	-	-	-	-	-	-	-	1.57	-
Ba	-	-	-	-	-	-	-	-	-	-	-	-	-	0.15	-
X_{Na}									0.14	0.18	0.06	0.69	0.53		
X_{Mg}	0.81	0.80	0.84	0.72	0.74	0.56	0.19	0.25	0.83	0.85	0.86			0.63	
X_{Ca}							0.28	0.20							

Supplementary Material

Fig. 1A

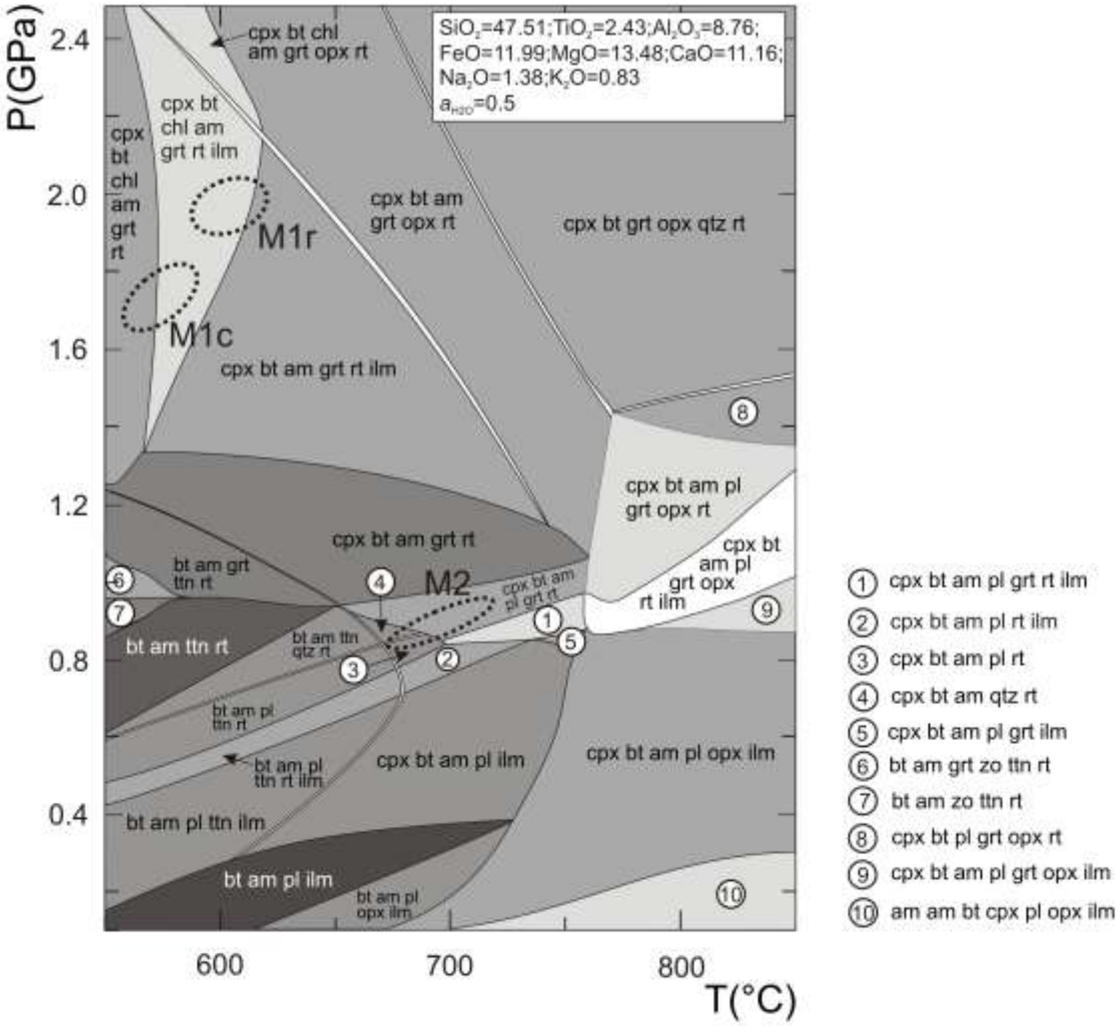

Fig. 2A

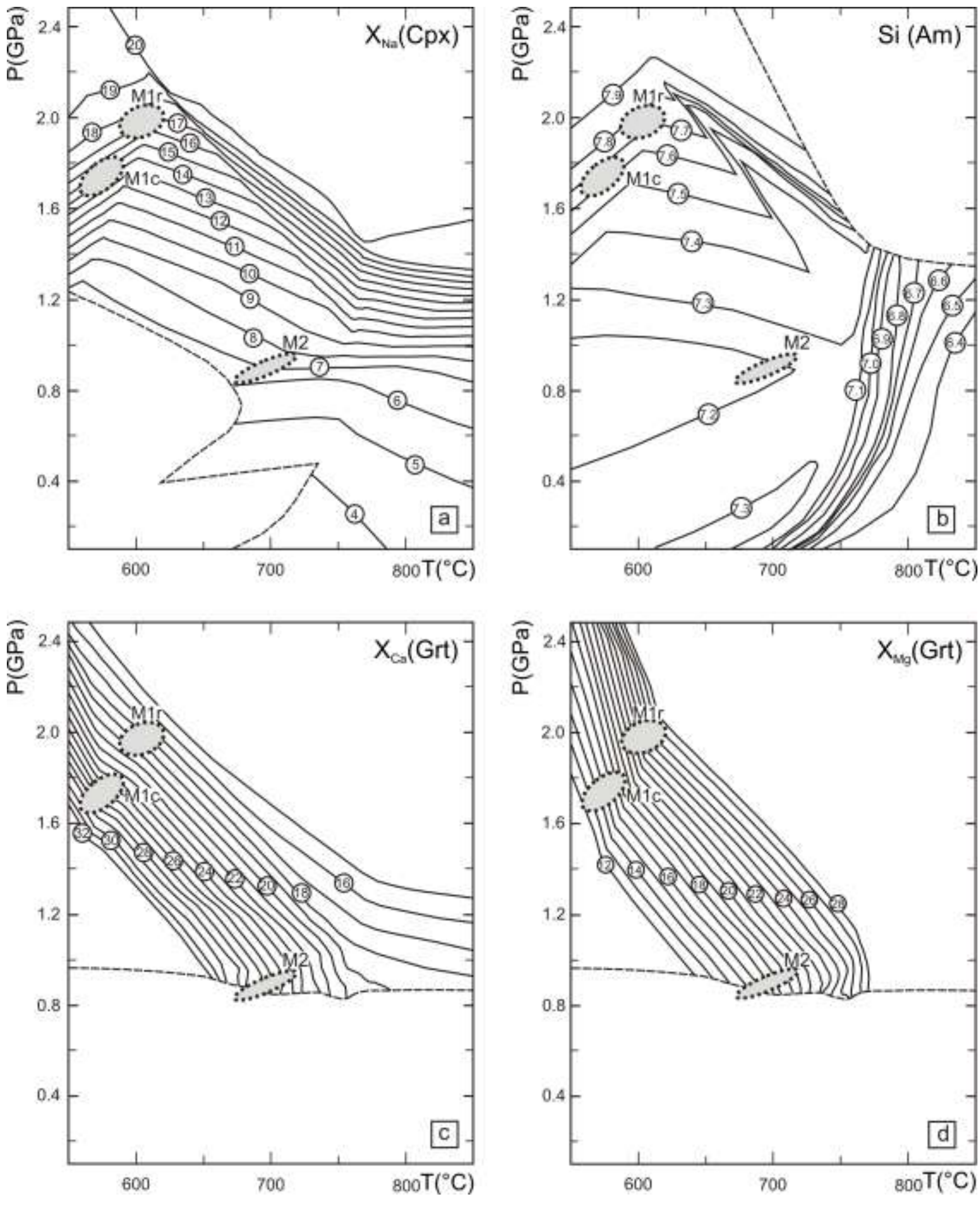

Table 1A

	U126	U126	u126	U126	U126	U126	U126	U126	U126	U126	U126	U126	U126	U126	U126
	$Am1_{core}$	$Am1_{rim}$	Am_2	Am_3	Grt_{core}	Grt_{rim}	$Cpx1_{core}$	$Cpx1_{rim}$	Cpx_2	Pl_1	Pl_2	Pl_3	Bt	Ilm	Ttn
SiO_2	52.55	52.07	44.46	44.81	38.39	37.47	53.69	54.46	53.53	57.63	55.02	67.47	34.59	0.04	29.26
TiO_2	0.49	0.47	0.95	1.53	0.10	0.01	-	0.06	0.04	0.09	0.03	-	5.07	53.73	38.94
Al_2O_3	3.80	4.68	12.47	11.86	22.57	22.18	2.60	2.93	2.01	27.21	28.30	20.14	14.70	-	0.92
Cr_2O_3	0.08	0.11	0.21	0.18	0.08	0.18	0.10	0.08	0.19	-	0.01	-	0.22	0.11	0.05
FeO	9.17	9.31	11.67	10.70	24.36	24.96	5.52	5.51	6.41	0.16	0.35	0.27	13.16	44.62	0.87
MnO	0.12	0.15	0.11	0.12	0.67	0.73	0.06	-	0.11	0.02	0.01	0.03	0.02	0.46	-
MgO	18.52	17.81	13.30	13.97	4.64	5.87	13.93	13.85	14.18	0.04	0.02	0.07	14.44	1.42	0.04
CaO	11.85	12.31	11.88	12.26	10.64	6.82	22.27	22.24	22.24	8.14	10.10	1.01	0.02	0.26	27.73
Na_2O	0.60	0.70	1.74	1.74	-	-	1.50	1.59	1.04	6.79	5.38	11.21	0.20	-	0.04
K_2O	0.19	0.24	0.77	0.81	-	-	-	-	-	0.14	0.10	0.06	7.92	0.02	-
BaO	-	-	-	-	-	-	-	-	-	-	-	-	3.23	-	-
F	0.13	0.28	0.09	0.21	-	-	-	-	-	-	0.09	0.11	0.16	-	0.19
Total	97.49	98.10	97.64	98.19	101.45	98.22	99.66	100.72	99.75	100.22	99.41	98.50	93.73	100.66	98.04
oxy	23	23	23	23	12	12	6	6	6	8	8	8	22	3	5
Si	7.43	7.36	6.47	6.49	2.94	2.96	1.97	1.98	1.97	2.57	2.49	2.95	5.36	-	0.98
Ti	0.05	0.05	0.10	0.17	0.01	-	-	-	-	-	-	-	0.59	1.00	0.98
Al	0.63	0.78	2.14	2.03	2.04	2.06	0.11	0.13	0.09	1.43	1.51	1.04	2.68	-	0.04
Cr	0.01	0.01	0.02	0.02	0.01	0.01	-	-	0.01	-	-	0.00	0.03	-	-
Fe^{2+}	0.72	0.80	1.21	1.18	1.51	1.65	0.12	0.14	0.17	0.01	0.01	0.01	1.70	0.92	0.02
Fe^{3+}	0.36	0.30	0.21	0.11	0.06	-	0.05	0.03	0.03	-	-	-	-	-	-
Mn	0.01	0.02	0.01	0.02	0.04	0.05	-	-	-	-	-	-	-	0.01	-
Mg	3.90	3.75	2.89	3.02	0.53	0.69	0.76	0.75	0.78	-	-	0.01	3.33	0.05	-
Ca	1.80	1.86	1.85	1.90	0.87	0.58	0.88	0.87	0.88	0.39	0.49	0.05	0.00	0.01	1.00
Na	0.16	0.19	0.49	0.49	-	-	0.11	0.11	0.07	0.59	0.47	0.95	0.06	-	-
K	0.03	0.04	0.14	0.15	-	-	-	-	-	0.01	0.01	-	1.56	-	-
Ba	-	-	-	-	-	-	-	-	-	-	-	-	0.20	-	-
X_{Na}							0.11	0.11	0.08	0.60	0.49	0.95			
X_{Mg}	0.84	0.82	0.71	0.72	0.18	0.23	0.87	0.84	0.83				0.66		
X_{Ca}					0.30	0.19									

Table 2A

	PO6	PO6	PO6	PO6	PO6	PO6	PO6	PO6	PO6	PO6	PO6	PO6	PO6
	$Am1_{core}$	$Am1_{rim}$	Am_2	Grt_{core}	Grt_{rim}	$Cpx1_{core}$	$Cpx1_{rim}$	Cpx_2	Pl_1	Pl_2	Pl_3	Bt	Ilm
SiO_2	54.37	50.01	44.72	38.52	38.70	54.50	54.58	53.58	57.77	54.31	66.58	35.52	0.05
TiO_2	0.12	0.93	1.42	0.05	0.03	0.02	0.07	0.04	-	-	0.04	2.62	53.33
Al_2O_3	2.29	6.19	13.60	22.54	22.83	1.25	1.61	1.19	25.49	27.90	19.63	15.96	-
Cr_2O_3	0.02	0.10	0.66	0.10	0.15	0.17	0.17	0.12	0.07	-	-	0.16	0.09
FeO	9.28	9.89	11.10	22.85	26.04	5.84	5.85	5.96	0.12	0.35	0.26	14.13	45.38
MnO	0.01	0.07	0.04	0.73	0.96	0.08	0.10	0.10	0.04	-	-	0.09	0.83
MgO	18.70	16.79	12.33	4.85	6.52	14.85	14.52	14.51	-	0.03	0.14	15.27	0.14
CaO	11.63	11.38	11.57	11.24	6.25	23.52	23.14	22.55	7.09	10.04	0.40	0.01	0.02
Na_2O	0.20	0.91	1.62	-	-	0.99	1.10	0.85	7.28	5.81	11.09	0.15	-
K_2O	0.20	0.39	0.56	-	-	-	-	-	0.09	0.02	0.21	8.45	-
BaO	-	-	-	-	-	-	-	-	-	-	-	2.56	-
F	0.01	0.15	0.39	-	-	-	-	-	-	0.07	0.05	0.27	-
Total	96.83	96.81	98.01	100.88	101.48	101.21	101.13	98.90	97.95	98.53	98.40	95.20	99.84
oxy	23	23	23	12	12	6	6	6	8	8	8	22	3
Si	7.73	7.17	6.48	2.96	2.96	1.98	1.98	1.99	2.63	2.49	2.97	5.40	-
Ti	0.01	0.10	0.16	-	-	-	-	-	-	-	-	0.30	1.01
Al	0.38	1.05	2.32	2.04	2.05	0.05	0.07	0.05	1.37	1.51	1.03	2.86	-
Cr	-	0.01	0.08	0.01	0.01	0.01	0.01	-	-	-	-	0.02	-
Fe^{2+}	1.02	0.84	1.22	1.44	1.65	0.12	0.14	0.17	0.01	0.01	0.01	1.80	0.95
Fe^{3+}	0.09	0.35	0.12	0.03	0.02	0.06	0.04	0.02	-	-	-	-	-
Mn	-	0.01	0.01	0.05	0.06	-	-	-	-	-	-	0.01	0.02
Mg	3.96	3.59	2.66	0.56	0.74	0.80	0.79	0.81	-	-	0.01	3.46	0.01
Ca	1.77	1.75	1.80	0.93	0.51	0.91	0.90	0.90	0.35	0.49	0.02	-	-
Na	0.06	0.25	0.46	-	-	0.07	0.08	0.06	0.64	0.52	0.96	0.04	-
K	0.04	0.07	0.10	-	-	-	-	-	0.01	-	0.01	1.64	-
Ba	-	-	-	-	-	-	-	-	-	-	-	0.15	-
X_{Na}						0.07	0.08	0.06	0.65	0.51	0.98		
X_{Mg}	0.80	0.81	0.69	0.19	0.25	0.87	0.85	0.83				0.66	
X_{Ca}				0.31	0.17								

Appendix

Matrix of residuals for reaction (1)

SiO_2	0.0000	0.0000	0.0000	0.0000
TiO_2	0.0015	0.0000	-0.0002	-0.0013
$AlO_{1.5}$	0.0141	0.0003	-0.0016	-0.0121
CaO	0.0057	0.0001	-0.0007	-0.0049
$NaO_{0.5}$	-0.0286	-0.0006	0.0033	0.0245
MgO	-0.0043	-0.0001	0.0005	0.0037
Fe	-0.0005	0.0000	0.0001	0.0005

Matrix of residuals for reaction (2)

SiO_2	-0.0081	-0.0131	-0.0064	-0.0100	-0.0041	0.0041	0.0175	0.0094
TiO_2	-0.0006	-0.0010	-0.0005	-0.0008	-0.0003	0.0003	0.0013	0.0007
$AlO_{1.5}$	0.0056	0.0090	0.0044	0.0069	0.0028	-0.0028	-0.0121	-0.0064
CaO	0.0112	0.0181	0.0088	0.0139	0.0057	-0.0056	-0.0242	-0.0129
$NaO_{0.5}$	0.0160	0.0257	0.0125	0.0198	0.0081	-0.0080	-0.0345	-0.0184
MgO	0.0048	0.0077	0.0037	0.0059	0.0024	-0.0024	-0.0103	-0.0055
Fe	0.0012	0.0019	0.0009	0.0015	0.0006	-0.0006	-0.0026	-0.0014
H_2O	-0.0003	-0.0004	-0.0002	-0.0003	-0.0001	0.0001	0.0005	0.0003